9 Representation of IASCC-Resistant or –Susceptible Behavior of 304- and 316-Type Steels in Sulfur-Carbon Map

Typical in-service cracking of BWR core internal components occurs at >2 dpa and is characterized by a virtually full intergranular fracture surface, sometimes accompanied by a small amount of transgranular fracture surface. In this respect, the IASCC behavior of SSs at ≈3 dpa (Section 8) is more relevant than that at ≈1.3 dpa (Section 7). As described in Section 8, IASCC-resistant or -susceptible behavior at ≈ 3 dpa is largely determined by the bulk concentrations of S and C. Similar analysis was performed for data reported in the literature. Virtually all literature data have been reported after 1987. Figures 42 and 43 show a two-dimensional map of bulk S and C contents to show the range in which 304- or 316-type steels are either resistant or susceptible to IASCC. The figure also includes similar data reported in the literature since 1987. The only data missing from the figure are those obtained for BWR internals for which S and C contents are not available, e.g., an IASCC-resistant 304 SS control blade sheath reported in Ref. 23 and an IASCC-susceptible 304L SS dry tube reported by Shen and Chang.[43]

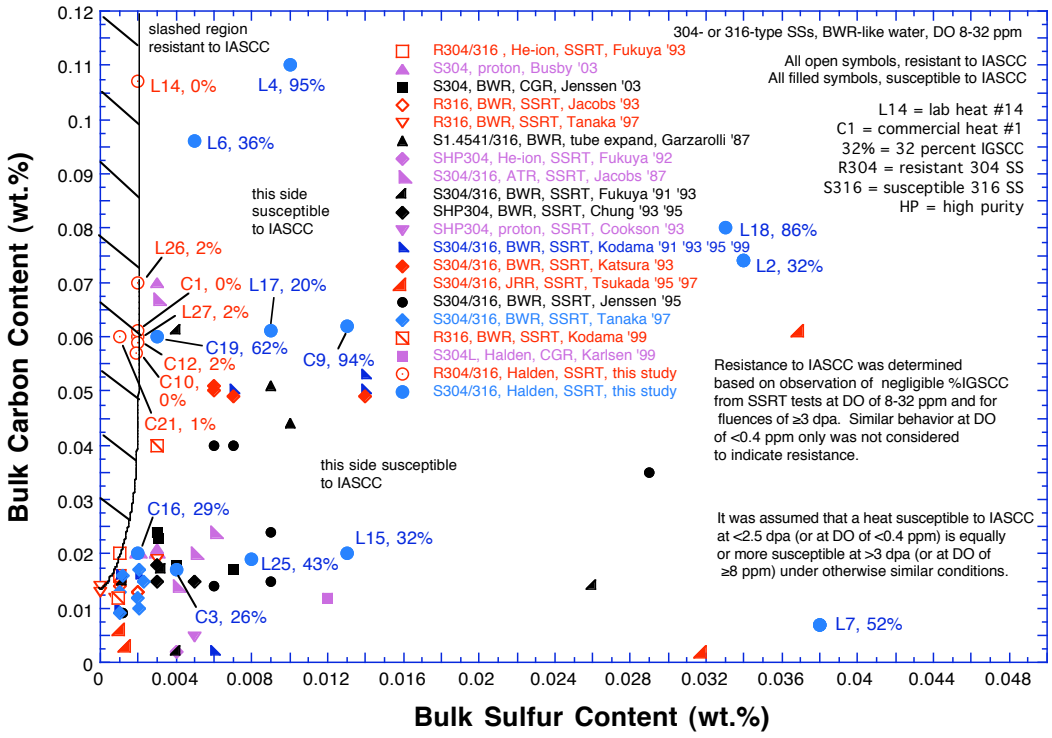

Figure 42. Range of bulk S and C contents in which Type 304 or 316 steels are resistant or susceptible to IASCC in BWR-like oxidizing water.

In constructing the maps in Figs. 42 or 43, it was assumed that a heat susceptible at <2.5 dpa is equally or more susceptible at ≥3 dpa under otherwise similar conditions. It was also assumed that a heat susceptible at a DO concentration of <0.4 ppm is more susceptible at a DO concentration of ≥8 ppm under otherwise identical conditions. Note that, in the figure, the plotted ranges of S and C contents extend beyond the AISI limits specified for Types 304 and 316 SS, i.e., maximum S, 0.030 wt.% and maximum C, 0.08 wt.%.

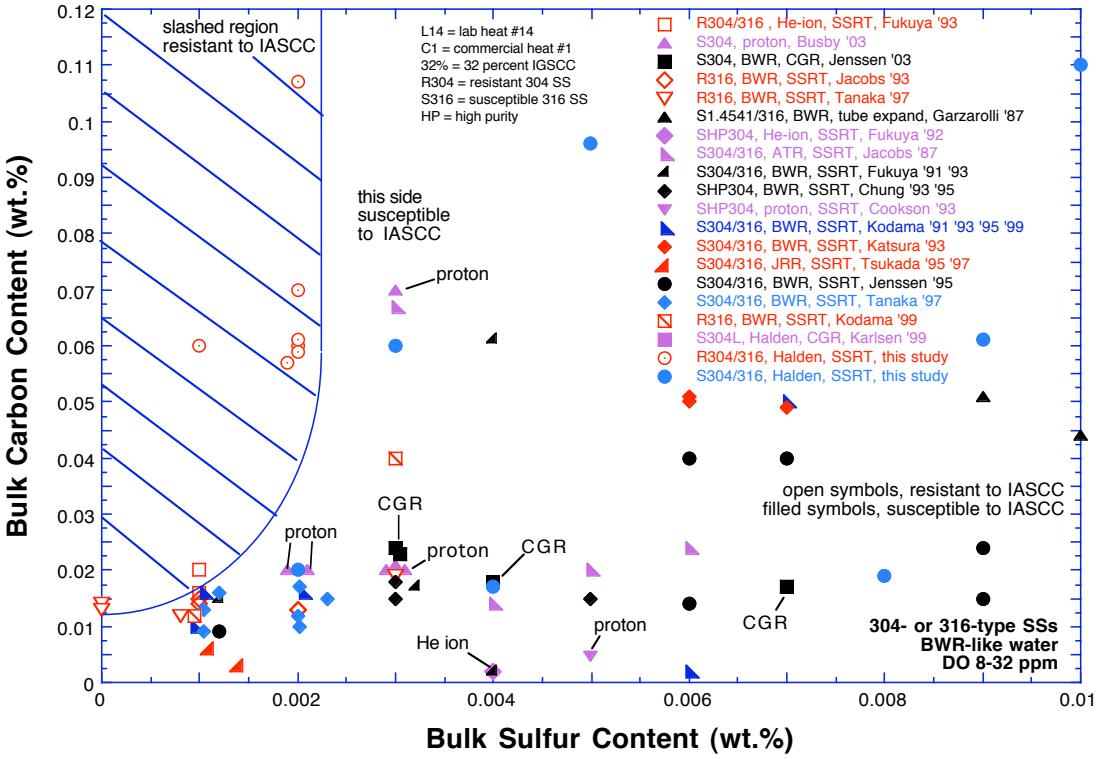

Figure 43. Expanded view of low-S portion of Fig. 42 showing data in detail.

In Figs. 42 and 43, data obtained on neutron-, ion-, or proton-irradiated steels from SSRT, crack-growth-rate (CGR), or tube-expansion tests are shown for comparison with those obtained by SSRT in this investigation. As shown in Fig. 43, the results obtained on He-ion-irradiated steels (Fukuya et al.[3]) and proton-irradiated steels (Cookson et al.[44] and Busby et al.[45]) are also consistent with the IASCC-susceptible range shown in the S-C map. The earlier efforts by the latter group of investigators focused on "ultra-high-purity" (UHP) heats. However, their "UHP" heats contained either insufficiently low concentrations of S, insufficiently high concentrations of C, or both, to render the steel resistant to IASCC. Figure 43 also includes the results of CGR tests reported by Karlsen and Hauso[46] and Jenssen et al.,[12] in which intergranular crack propagation was confirmed by SEM fractography.

In Fig. 44, which is similar to Fig. 42, data points for four susceptible heats tested after irradiation to 1.3 dpa (i.e., Heats L22, L11, L13, and L8; see Fig. 29) are also included. It was assumed that the four heats are also susceptible to IASCC at 3 dpa, although they were not tested at this damage level.

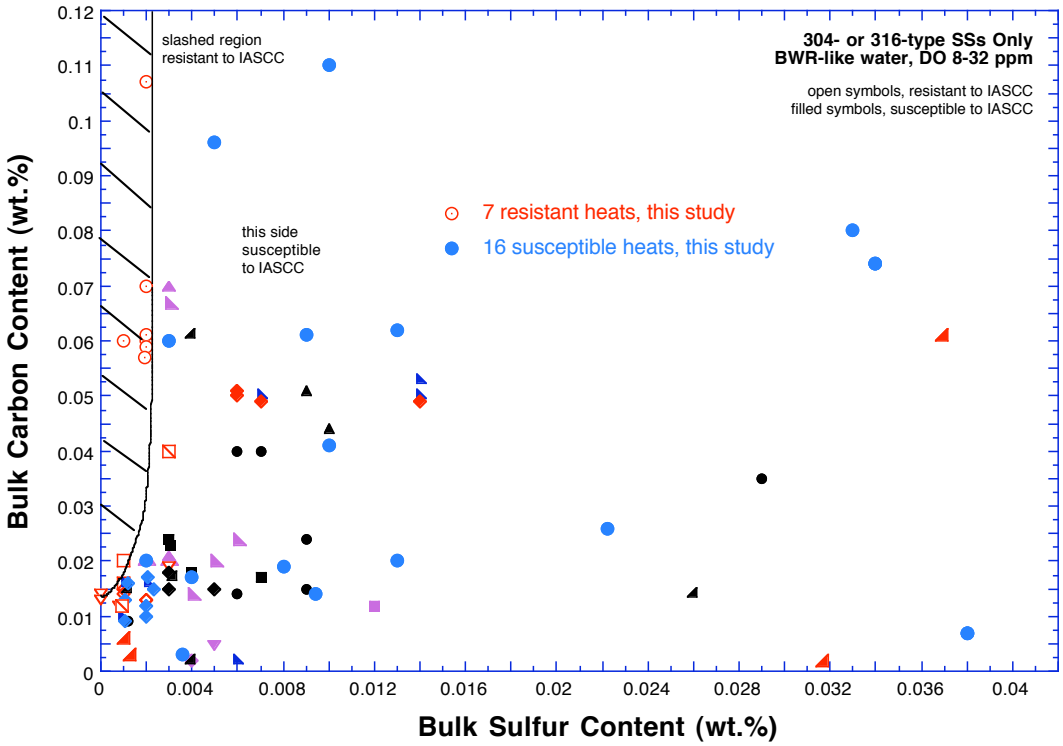

Figure 44. Range of bulk S and C contents in which Type 304 or 316 steels are resistant or susceptible to IASCC, including four susceptible heats tested at 1.3 dpa in this study.

This page is intentionally blank.

10 IASCC Behavior of Type 348 Steels

Besides the 304- and 316-type steels, two heats of 348-type SS were tested in 289°C water in this investigation after irradiation to ≈1.3 and ≈3 dpa. One heat (L23) contains a very high concentration of S (0.0475 wt.%) and the other (L24), a low concentration of S (0.0055 wt.%). Percent IGSCC of the two heats is compared in Fig. 45. The high-S heat was susceptible to IASCC, but the low-S heat was resistant at both levels of neutron damage. This behavior is consistent with the behavior of 304- or 316-type SSs described in Section 8.

Similar to the correlation established for 304- and 316-type SSs in Fig. 42, the IASCC-resistant range of 348-type and an Nb-containing SS was plotted in a two-dimensional S-C map in Fig. 46. This map includes all such data in the literature that were obtained under BWR- and PWR-like conditions. As indicated in the figure, it appears that the IASCC-resistant range of 348-type and Nb-doped SSs in PWR- or BWR-like water can be described well in an S-C map that differs somewhat from S-C map of 304- and 316-type SSs. Behavior of the Nb-doped 316-type steel was reported by Jacobs et al. for BWR conditions.[21] Although the correlation in Fig. 46 should be considered only preliminary, it is qualitatively consistent with the correlation constructed for 304- and 316-type SS for BWR-like conditions. It appears that 348-type SSs exhibit higher tolerance to S than 304- or 316-type steels.

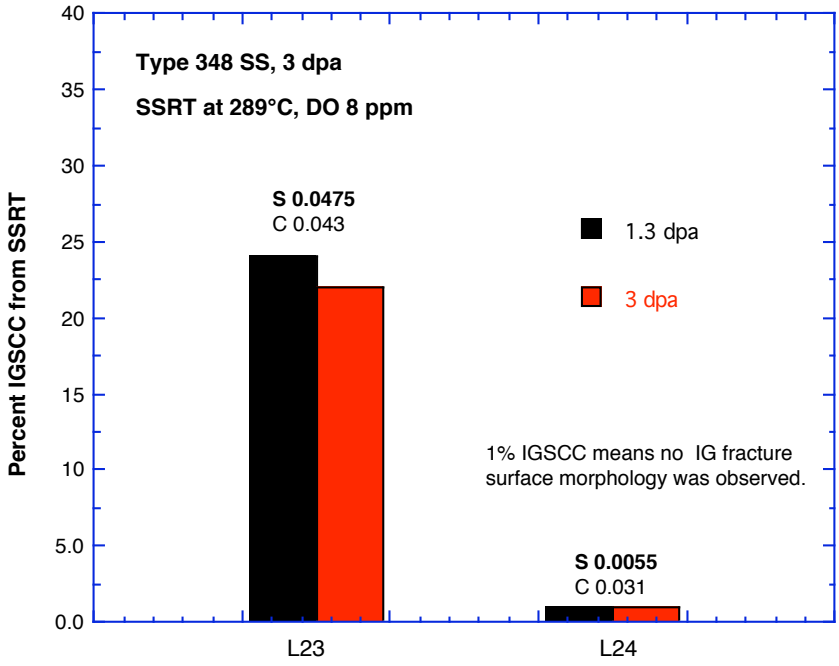

Figure 45. Percent IGSCC of high- and low-sulfur laboratory heats of Type 348 SS after irradiation to 1.3 and 3 dpa, SSRT test in BWR-like water.

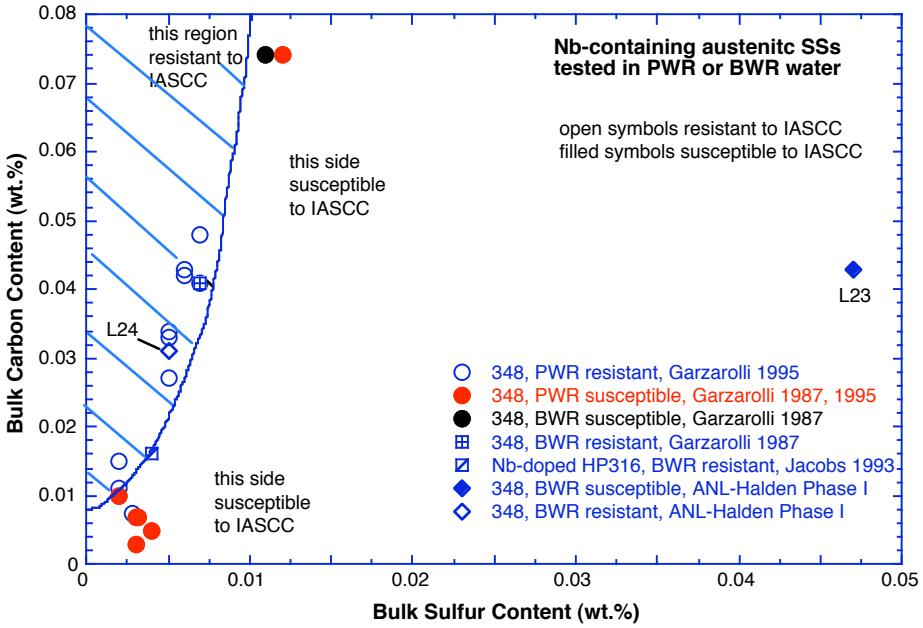

Figure 46.
Range of bulk S and C contents in which Type 348 stainless steels are resistant or susceptible to IASCC.

11 IASCC Behavior of Austenitic-Ferritic Steel

In this investigation, one austenitic-ferritic duplex SS alloy was tested by SSRT in 289°C water after irradiation to 0.4, 1.3, and 3.0 dpa. The alloy (L5), which contains 21 wt.% Cr and ≈3 vol.% delta ferrite, was resistant to IASCC, even though its S content was very high (i.e., 0.028 wt.%). Figure 47 shows an insignificant level of percent IGSCC measured on the alloy at all the three damage levels.

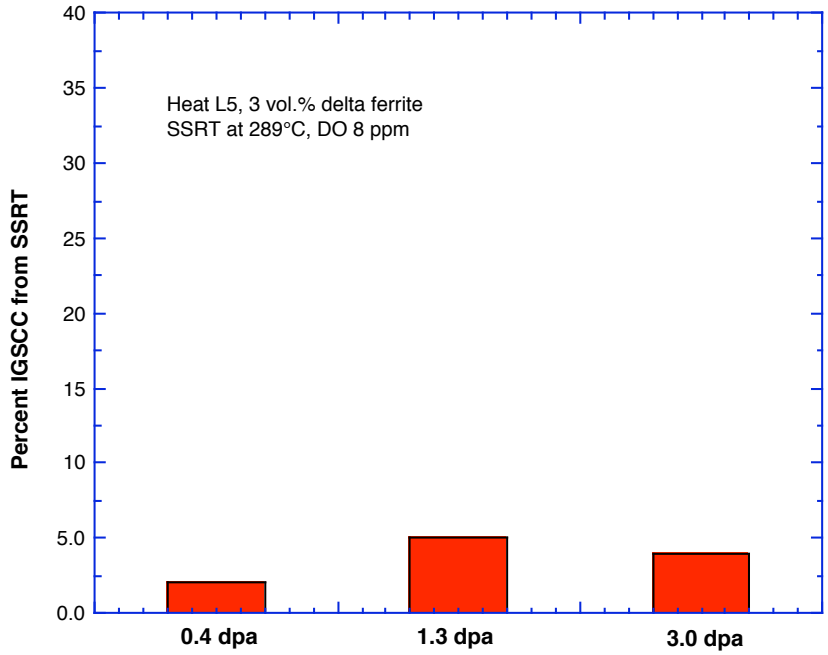

Figure 47. Effect of neutron damage on percent IGSCC of austenitic-ferritic steel (Heat L5) that contains ≈3 vol.% delta ferrite.

The morphology of the delta ferrite in the alloy was globular, as shown in Fig. 48. Annealing twins are also visible in the optical metallograph. The fracture surface of the alloy at 3 dpa showed small broken islands of delta ferrite surrounded by dominantly ductile regions (see Fig. 49).

The excellent resistance of this alloy to IASCC appears to be consistent with the behavior of cast austenitic SSs of Types CF-3 and CF-8, which, in the unirradiated state, are well known for their resistance to IGSCC. Most CF-3 and CF-8 duplex SSs contain a delta ferrite content of >10 vol.%, usually in the form of acicular or elongated grains. If the volume fraction of delta ferrite is too high, or if the distribution of ferrite is continuous, significant embrittlement due to ferrite cleavage may lead to unacceptable degradation of fracture toughness after irradiation to high fluence. However, with a ferrite content of only ≈3%, as in Alloy L5, small globular ferrite islands remain isolated, and overall material embrittlement due to ferrite cleavage appears insignificant. Supporting this premise, yield strength and total elongation of the alloy in 289°C water were significant even after irradiation.

It appears that the mechanism through which a small amount of delta ferrite may suppress the susceptibility to IASCC in Alloy L5 can be explained well by the effect of delta ferrite on S distribution in the steel. As shown in the equilibrium Fe-S diagram in Fig. 50, the solubility limit of S is several times higher in the δ ferrite phase than in the austenitic (γ) phase. At ≈1365°C, the solubility limits of S in delta ferrite and austenite are 0.18 and 0.05 wt.%, respectively. Therefore, during ingot melting, solidification, and cooling of

a material such as L5, S atoms are expected to migrate toward and be incorporated into the delta ferrite globules, which act as efficient trapping sites for S atoms. As a result, segregation of S atoms to austenite grain boundaries during fabrication or irradiation will be suppressed because of the presence of ferrite globules and the large austenite-ferrite phase boundaries.

Also, continuous austenite grain boundaries are rare in this type of steel, because ferrite grains intersect austenite grain boundaries. As a consequence, continuous crack propagation along austenite grain boundaries seems to be more difficult, and, as a consequence, IASCC susceptibility seems to be suppressed significantly.

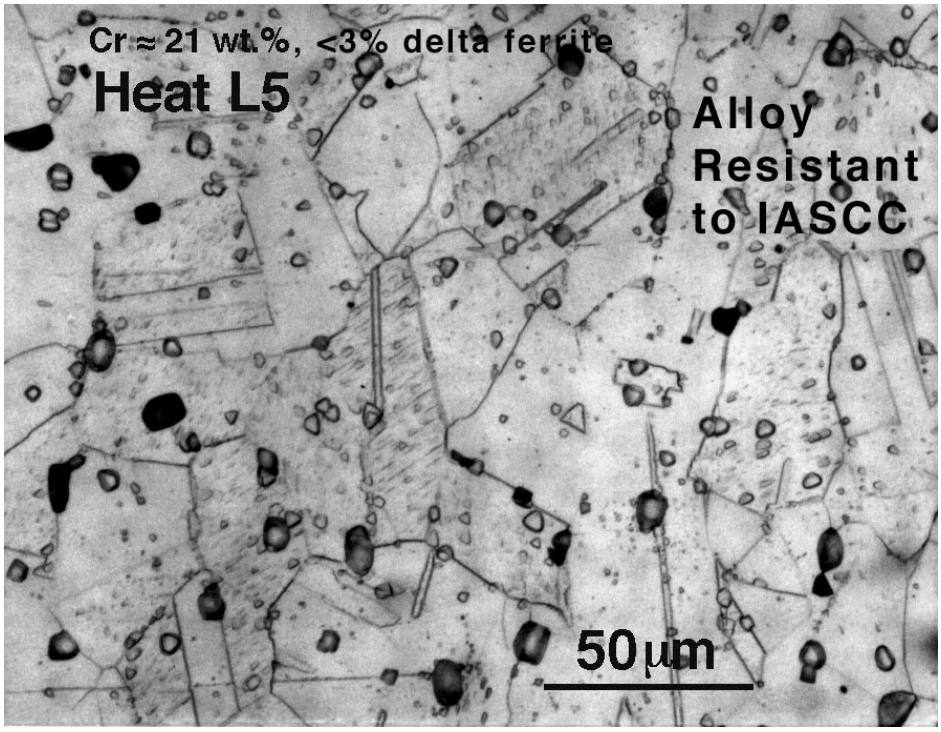

Figure 48.
Optical metallograph of IASCC-resistant Alloy L5 that contains ≈3 vol.% delta ferrite.

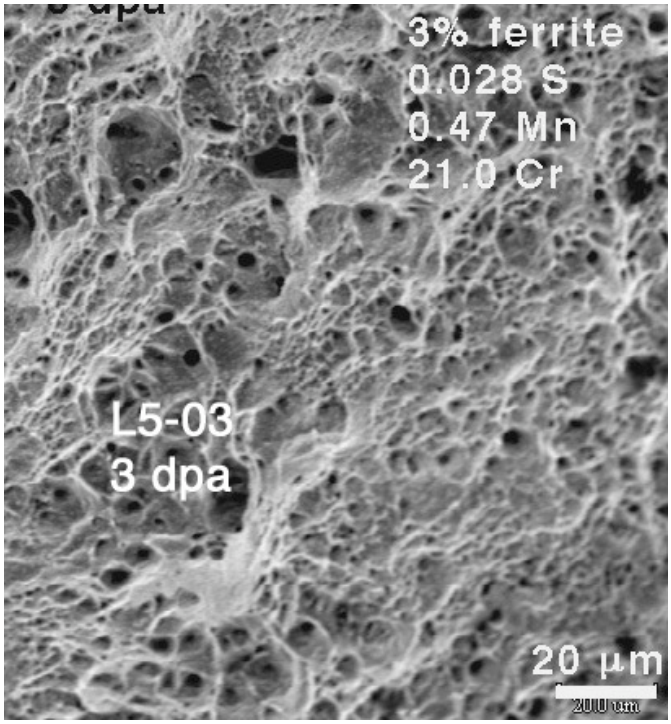

Figure 49.
Predominantly ductile fracture surface morphology of IASCC-resistant Alloy L5 that contains ≈3 vol.% delta ferrite, 3 dpa.

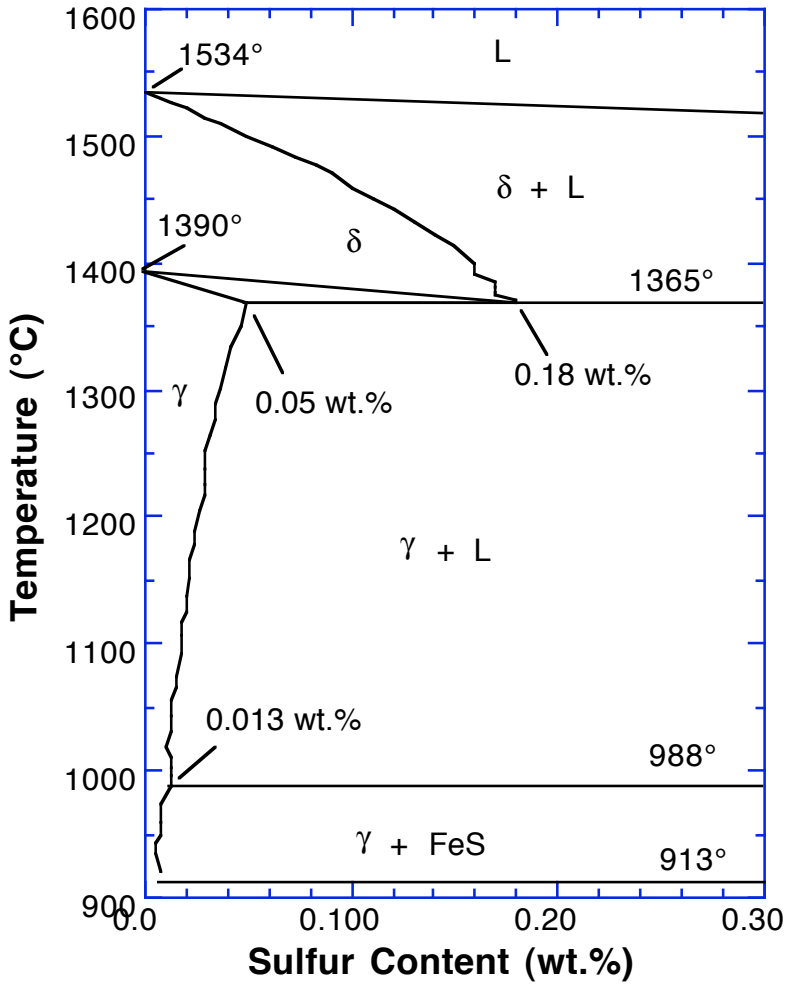

Figure 50.
Fe-rich side of Fe-S phase diagram; from Hansen, Ref. 47.

This page is intentionally blank.

12 Fractographic Analysis

Fractographs produced in 289°C water were obtained in a shielded SEM for all 3-dpa specimens listed in Table 14. Fractographs were also obtained for specimens that were irradiated to 0.4 and 1.3 dpa; some of these specimens exhibited significant susceptibility to IASCC. Typically, 10-15 fractographs were obtained for each specimen at various magnifications ranging from 20X to 800X. For each specimen, a composite fractograph was then constructed for the whole fracture surface at a magnification ranging from 100X to 150X. This section summarizes results of the fractographic analysis for 3-dpa specimens.

12.1 Fracture Surface Morphology of IASCC-Resistant Heats of 304, 316, and 348 Type Steels at 3 dpa

Typical fracture surface morphologies of the IASCC-resistant seven heats of 304- or 316-type SSs (see Fig. 28) and one heat of 348 SS (see Fig. 45) are shown in Figs. 51-58. All of the eight heats, which were irradiated to 3 dpa, exhibited predominantly ductile fracture surface morphology, sometimes mixed with a limited amount of transgranular fracture. Percent intergranular fracture was negligible in the eight heats (i.e., ≤2%).

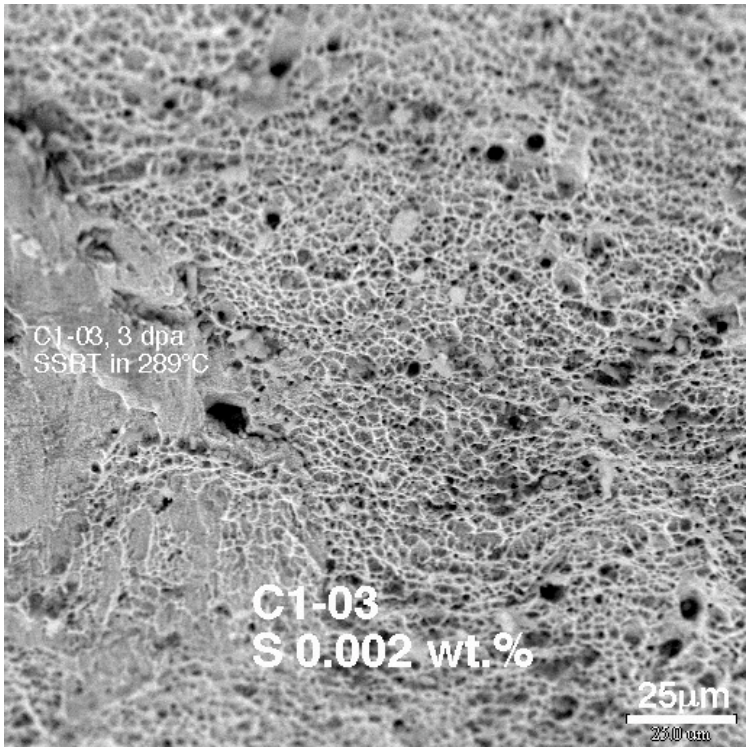

Figure 51.
Dominantly ductile fracture surface morphology of IASCC-resistant Commercial Heat C1 of Type 304 SS; 3 dpa.

Transgranular fracture morphology was often observed near the specimen free surfaces, which were covered with thin oxide layers. In the IASCC-resistant heats, a transition from transgranular morphology to ductile morphology was often observed not far from the specimen free surface. Such examples are visible in Figs. 51, 56, and 57. The fracture surface morphology of Laboratory Heat L26 (Fig. 57) shows

predominantly ductile morphology and a limited amount of transgranular morphology that surrounds an insignificant amount of intergranular morphology of ≈2%.

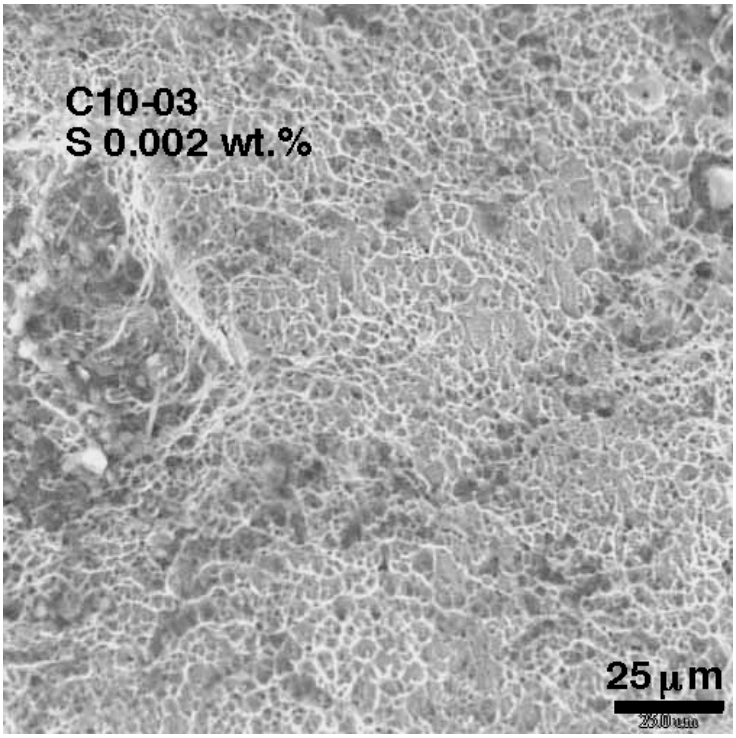

Figure 52. Dominantly ductile fracture surface morphology of IASCC-resistant Commercial Heat C10 of Type 304 SS; 3 dpa.

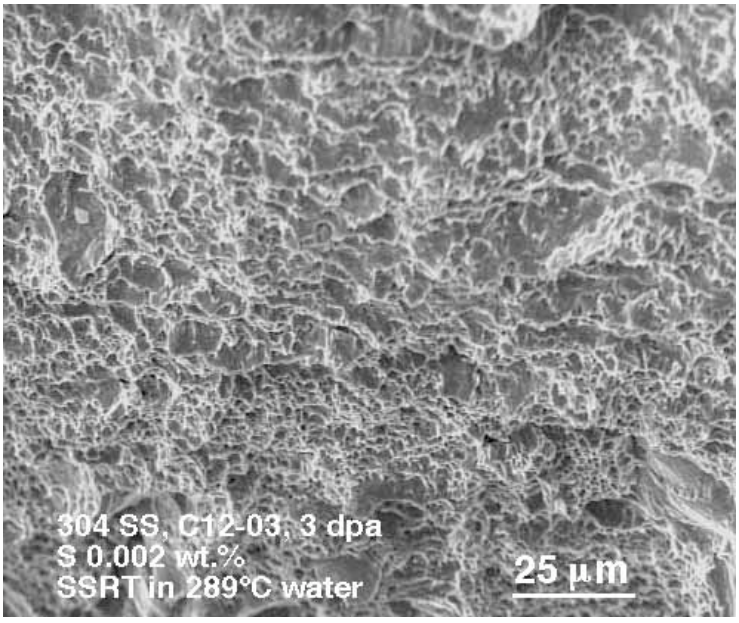

Figure 53. Dominantly ductile fracture surface morphology of IASCC-resistant Commercial Heat C12 of Type 304 SS; 3 dpa.

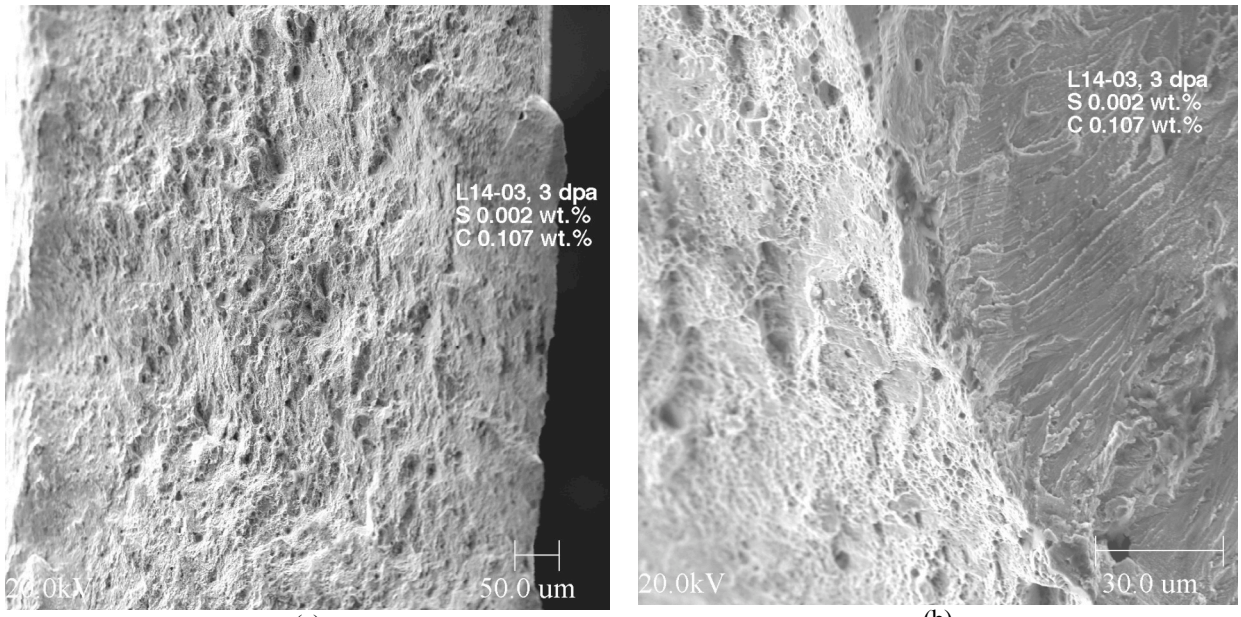

(a) (b)

Figure 54. Fracture surface morphology of IASCC-resistant Laboratory Heat L14 of Type 304 SS (3 dpa), showing predominant ductile morphology (a) and limited transgranular morphology (b); intergranular morphology is negligible.

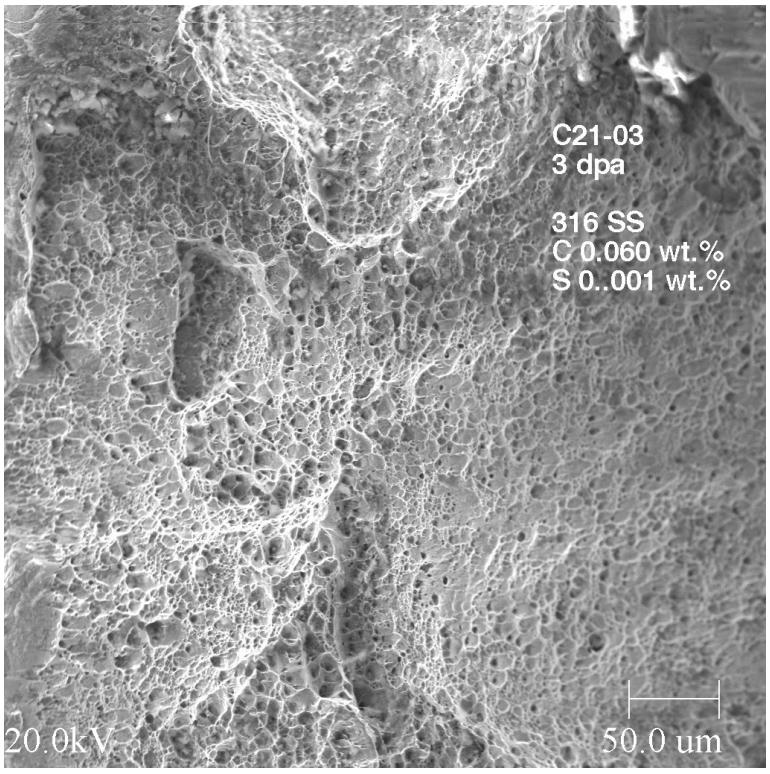

Figure 55. Dominantly ductile fracture surface morphology of IASCC-resistant Commercial Heat C21 of Type 316 SS; 3 dpa.

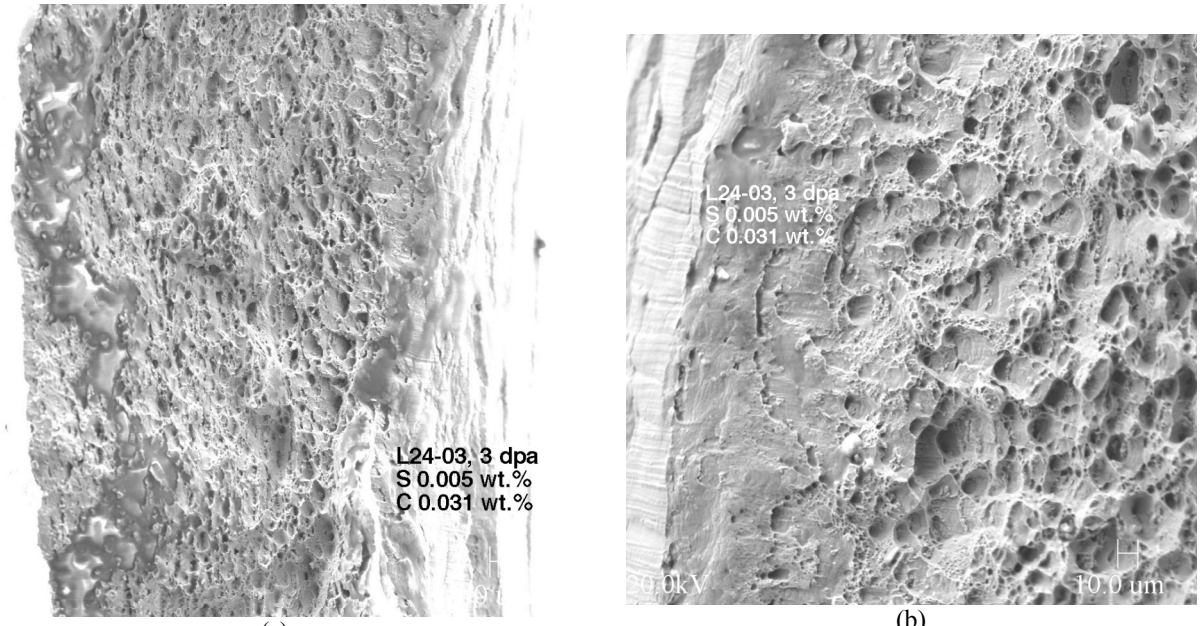

(a) (b)

Figure 56. Fracture surface morphology of IASCC-resistant Laboratory Heat L24 of Type 348 SS (3 dpa); both low- (a) and high-magnification (b) images show that ductile morphology is dominant and intergranular morphology is negligible.

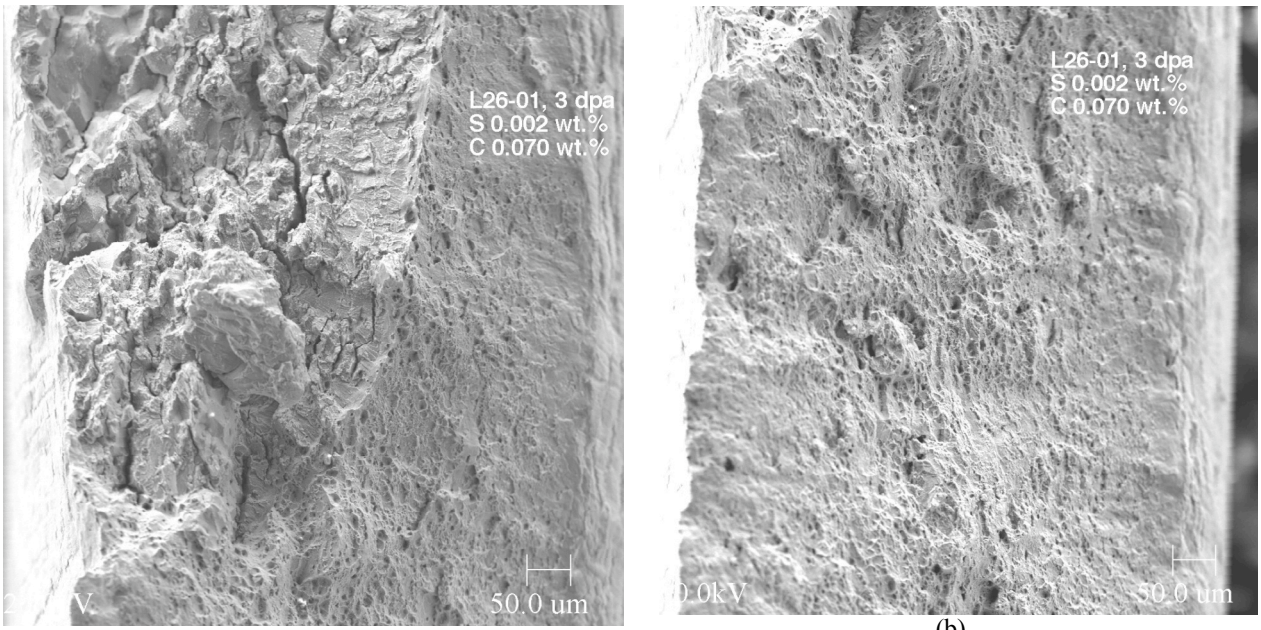

(a) (b)

Figure 57. Fracture surface morphology of IASCC-resistant Laboratory Heat L26 of Type 304 SS (3 dpa), showing (a) limited amount of transgranular morphology that surrounds insignificant amount of intergranular morphology (≈2% IGSCC) and (b) dominantly ductile morphology.

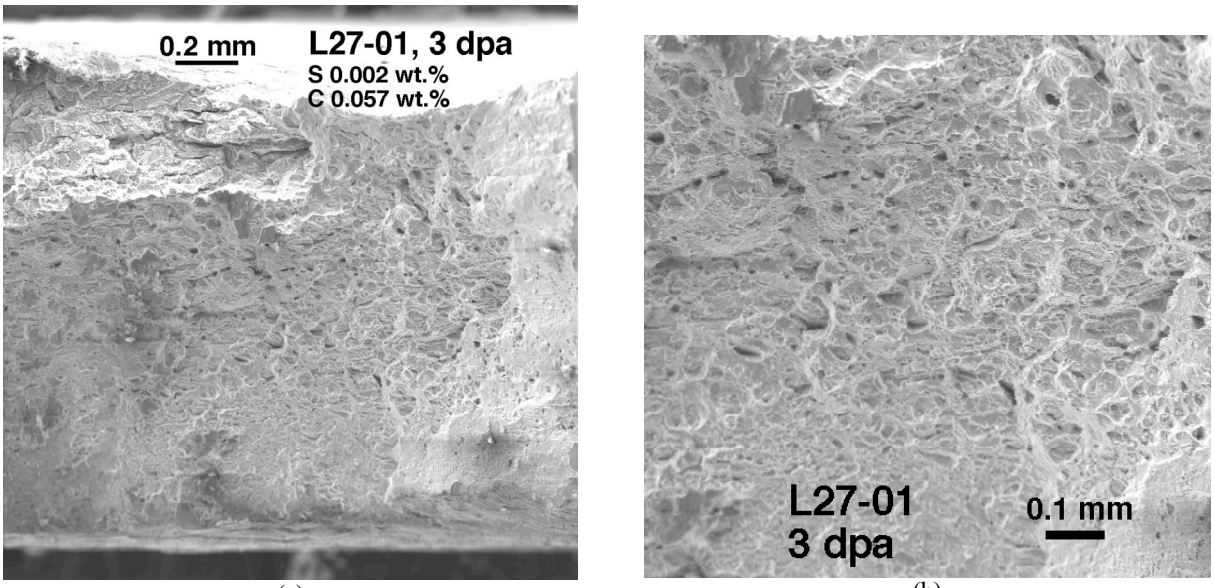

(a) (b)

Figure 58. Ductile fracture morphology of IASCC-resistant Laboratory Heat L27 (Type 316 SS, 3 dpa); both low- (a) and high-magnification (b) images show that intergranular morphology is negligible.

12.2 Fracture Surface Morphology of IASCC-Susceptible Heats of 304, 316, and 348 Type Steels at 3 dpa

Typical fracture surface morphologies of the 12 IASCC-susceptible heats of 304- or 316-type SSs (3 dpa) are shown in Figs. 59-70. Similar morphology for one susceptible 348 SS heat is shown in Fig. 71. All of the 13 heats exhibited a significant amount of intergranular fracture surface morphology, sometimes close to 100%. From the results of fractographic analysis, several characteristics were observed:

(1) Most of the intergranular fracture surfaces show numerous secondary cracks along the grain boundaries. These cracks branch at sharp angles from the plane of the main crack propagation.

(2) In some cases, virtually whole grains appear to be encircled by intergranular separation, e.g., Figs. 59, 60, 63, and 64. This phenomenon has been commonly referred to as "grain encirclement" by some investigators. Sometimes, such a grain "drops out," like a grain of sand, during metallographic polishing.

(3) Intergranular fracture surfaces are often covered with an unknown type of corrosion debris, e.g., Figs. 59, 60, 62, 63, 66, 67, 68, 70, and 71. The shape of the debris is mostly spherical, but in some case, it is tetrahedral, e.g., Fig. 62.

(4) Little corrosion debris is observed on ductile or transgranular fracture surfaces.

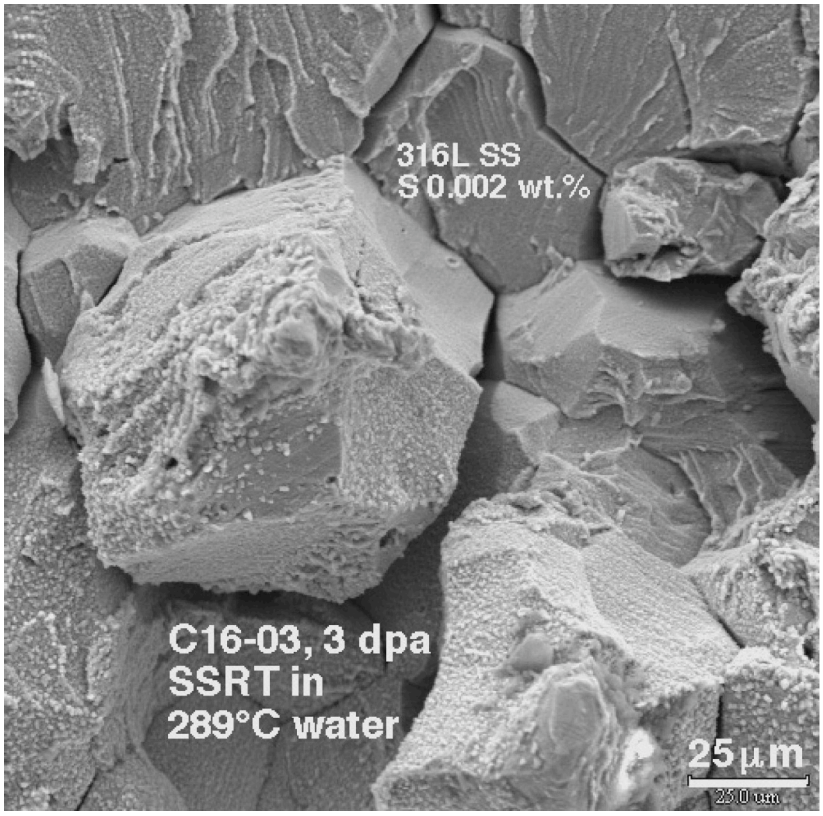

Figure 59.
Intergranular fracture surface morphology of IASCC-susceptible Heat C16 (316L SS, 3 dpa). Note secondary cracks along grain boundaries at high angles to plane of main crack propagation.

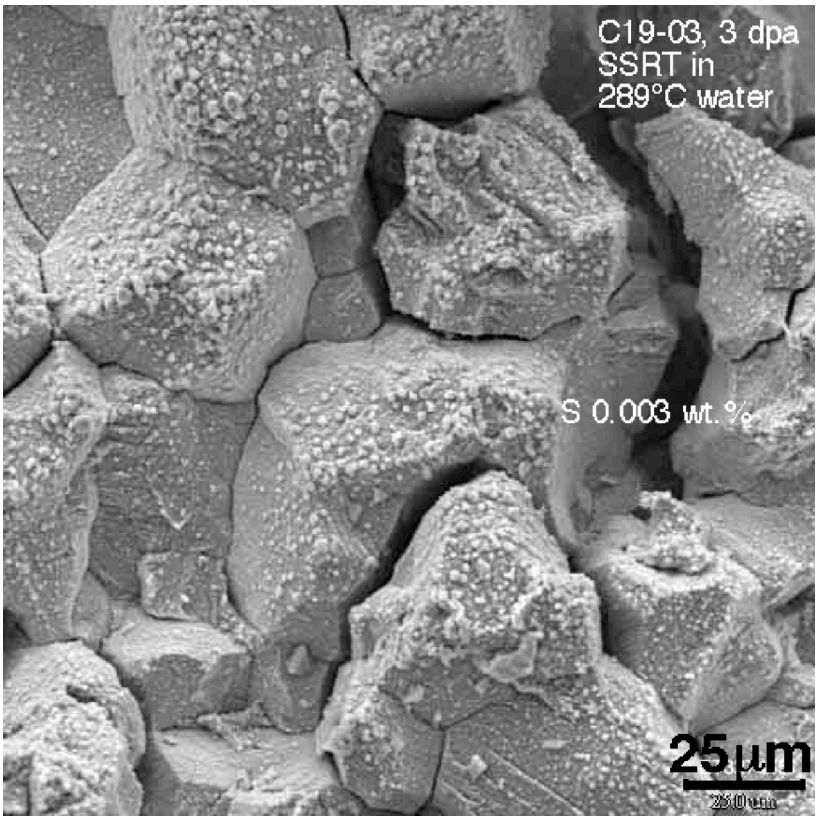

Figure 60.
Intergranular fracture surface morphology of IASCC-susceptible Heat C19 (304 SS, 3 dpa). Note corrosion debris and secondary cracks along grain boundaries at high angles to plane of main crack propagation.

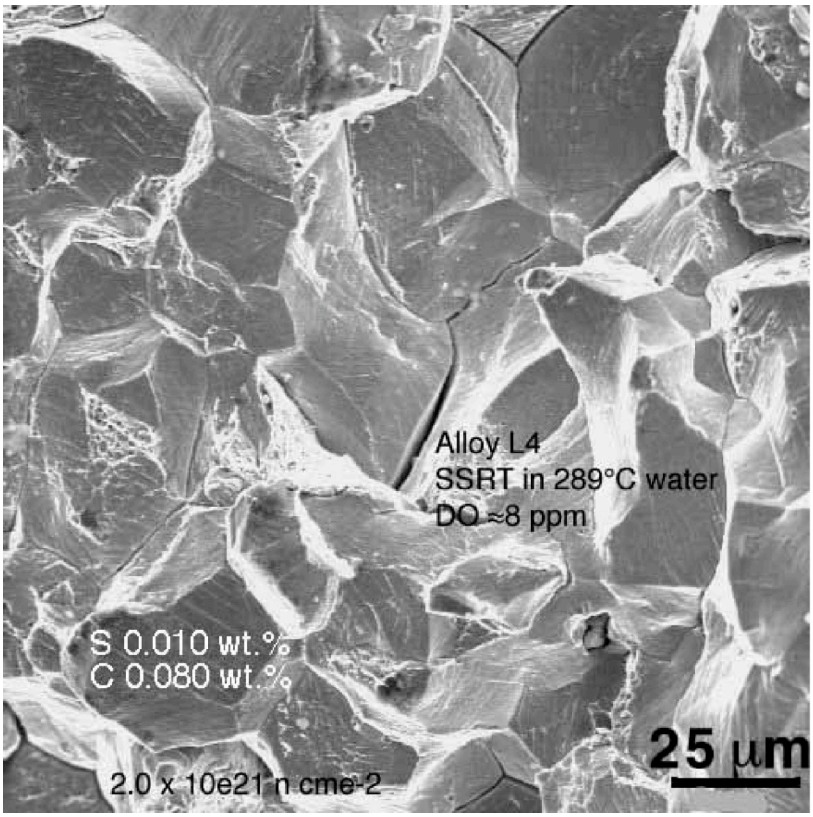

Figure 61.
Intergranular fracture surface morphology of IASCC-susceptible Heat L4 (304 SS, 3 dpa). Note secondary cracks along grain boundaries at high angles to plane of main crack propagation.

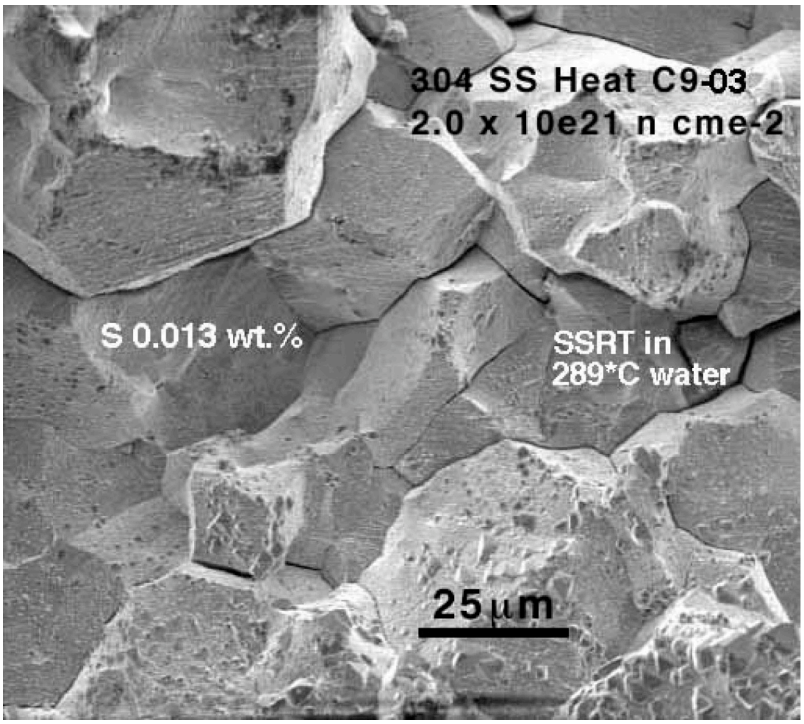

Figure 62.
Intergranular fracture surface morphology of IASCC-susceptible Heat C9 (304 SS, 3 dpa). Note corrosion debris and secondary cracks along grain boundaries at high angles to plane of main crack propagation.

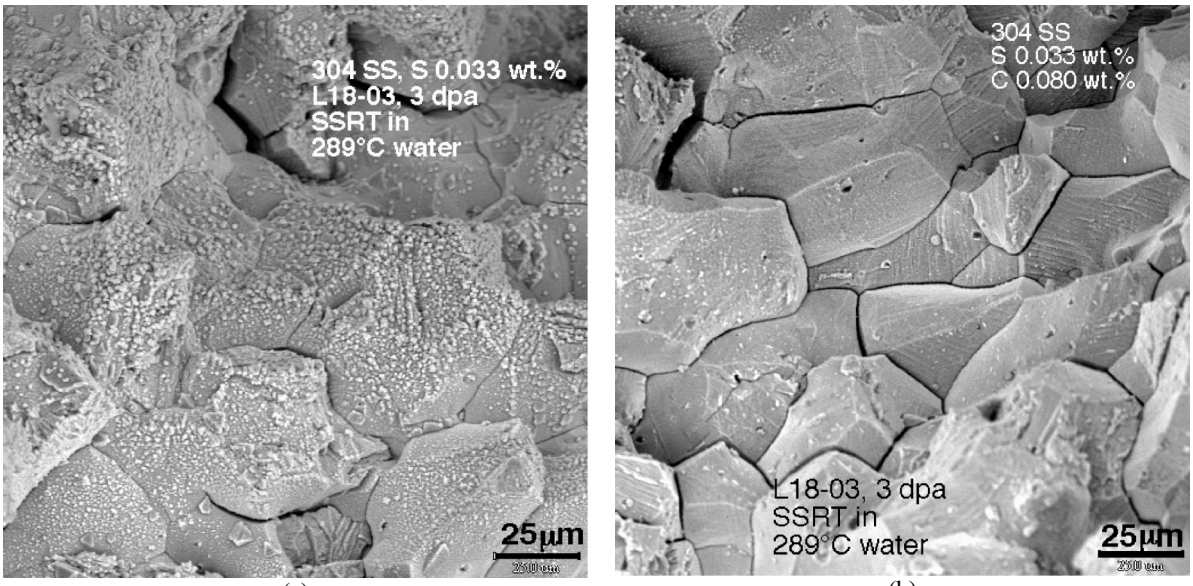

(a) (b)

Figure 63. Intergranular fracture surface morphology of IASCC-susceptible Heat L18 (304 SS, 3 dpa). Note corrosion debris and secondary cracks along grain boundaries at high angles to plane of main crack propagation.

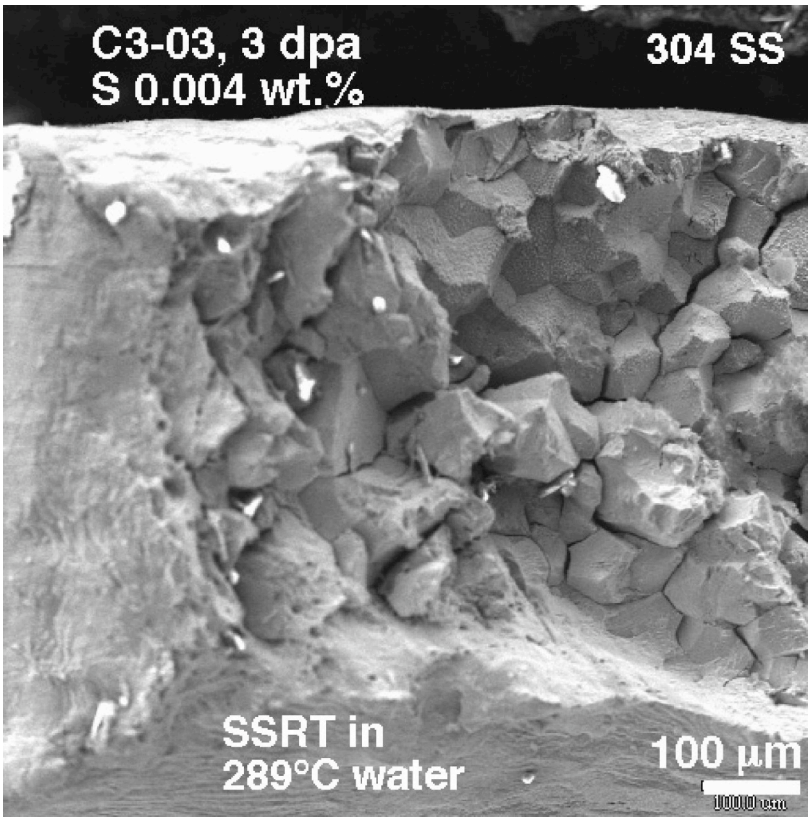

Figure 64. Intergranular fracture surface morphology of IASCC-susceptible Heat C3 (304L SS, 3 dpa). Note secondary cracks along grain boundaries.

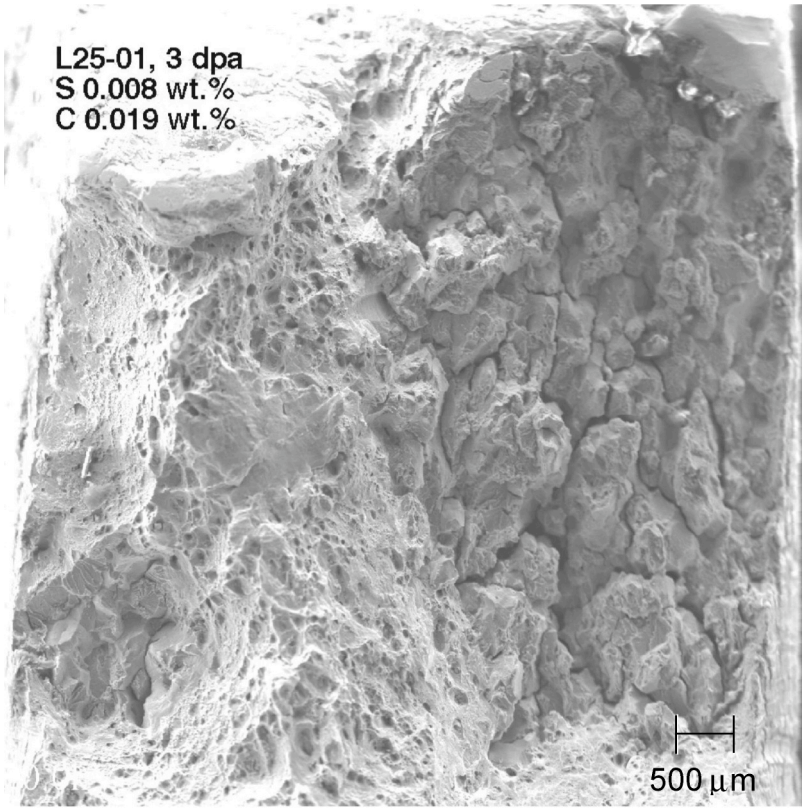

Figure 65. Intergranular and ductile fracture surface morphologies of IASCC-susceptible Heat L25 (304L SS, 3 dpa). Note secondary cracks along grain boundaries.

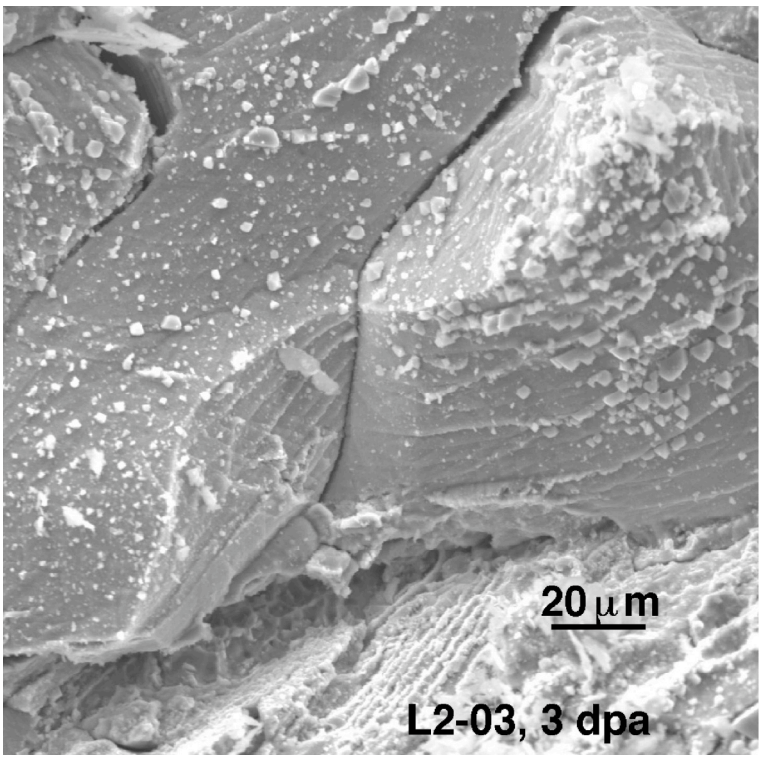

Figure 66. Intergranular fracture surface morphology of IASCC-susceptible Heat L2 (304 SS, 3 dpa). Note corrosion debris and deformation steps on grain boundaries.

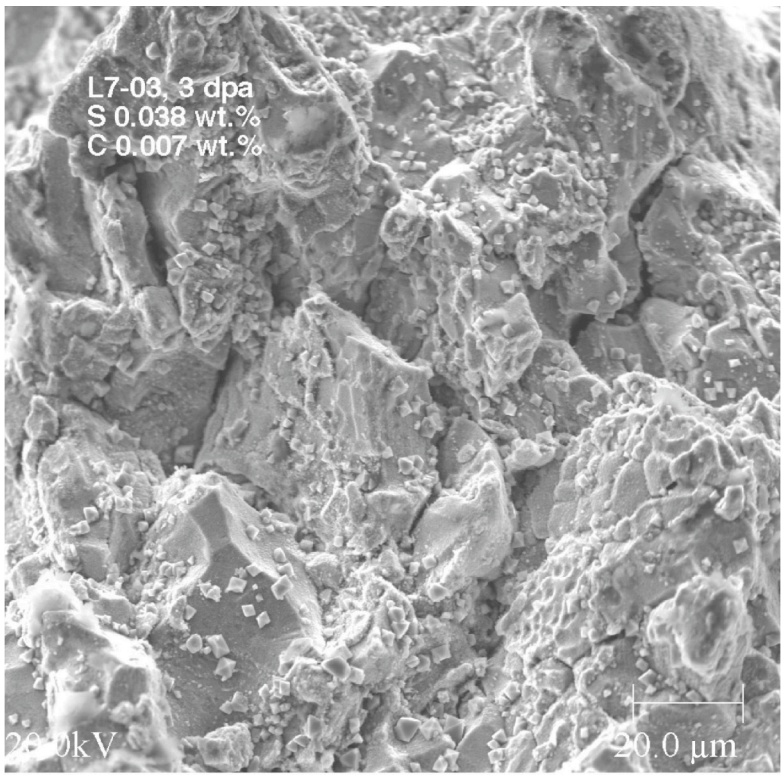

Figure 67. Intergranular fracture surface morphology of IASCC-susceptible Heat L7 (304L SS, 3 dpa). Note corrosion debris and high-angle secondary cracks.

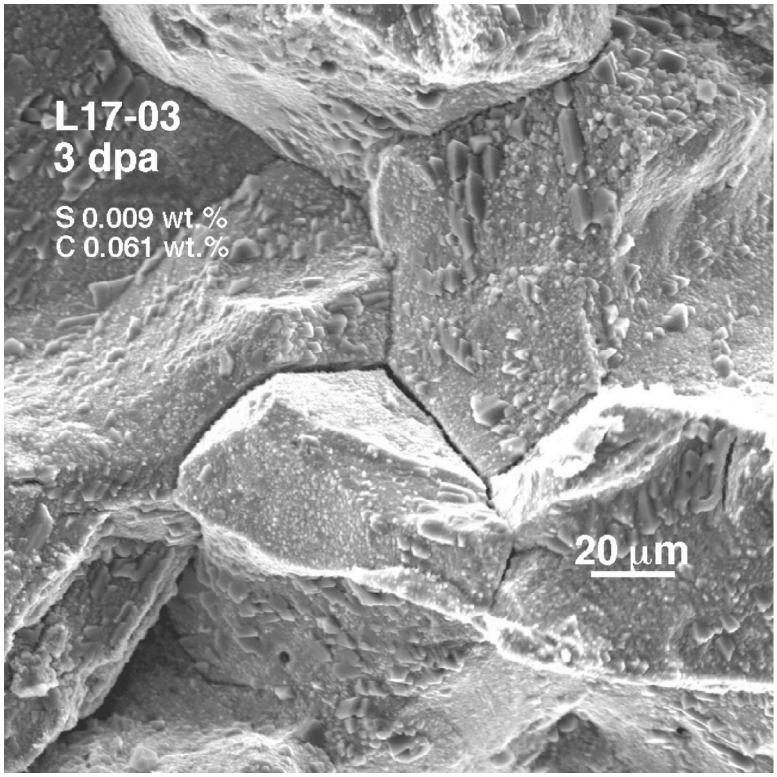

Figure 68. Intergranular fracture surface morphology of IASCC-susceptible Heat L17 (304 SS, 3 dpa). Note corrosion debris and high-angle secondary cracks.

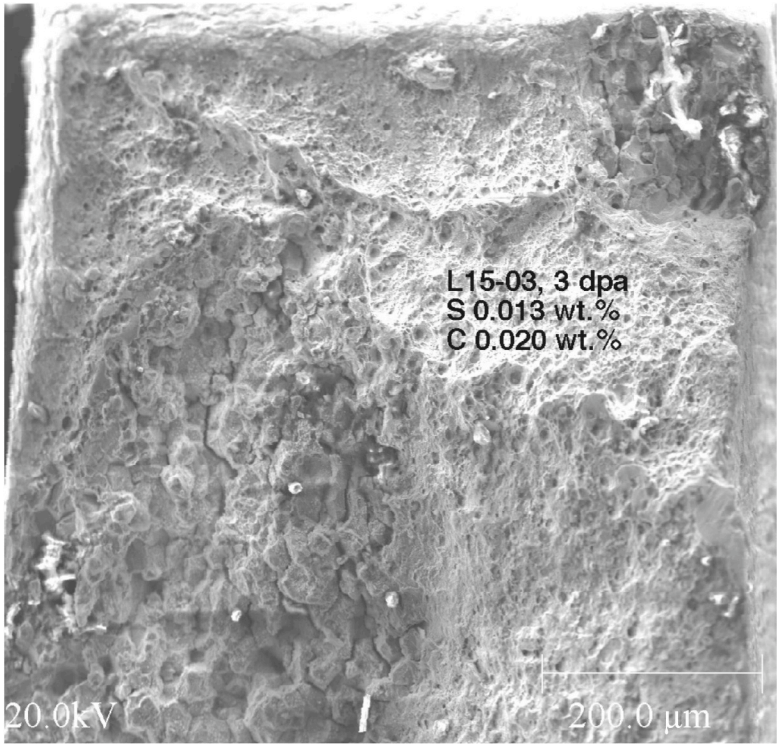

Figure 69. Intergranular and ductile fracture surface morphologies of IASCC-susceptible Heat L15 (304L SS, 3 dpa).

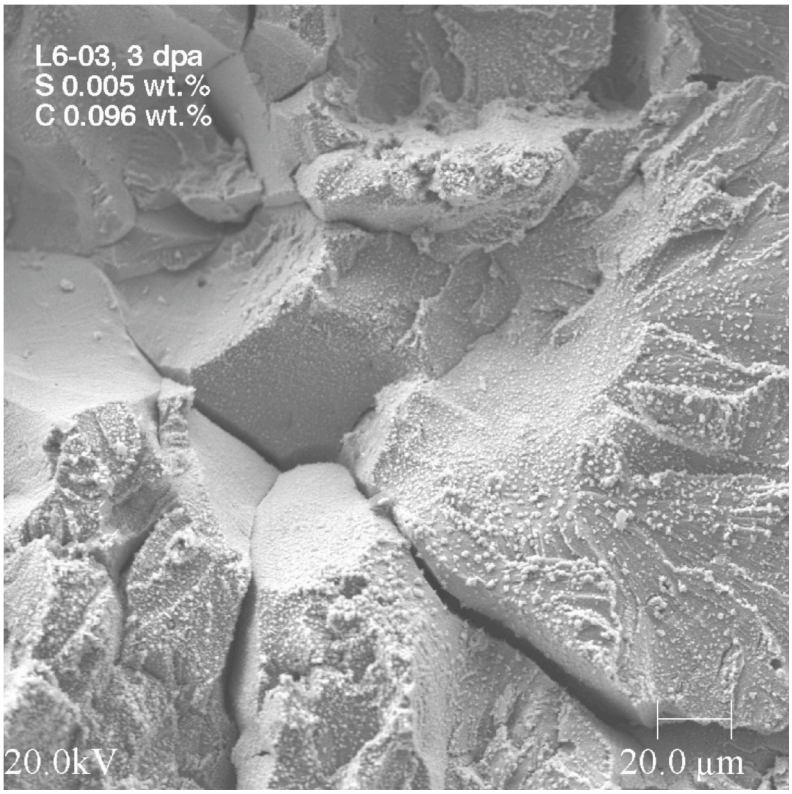

Figure 70. Intergranular fracture surface morphology of IASCC-susceptible Heat L6 (304 SS, 3 dpa). Note corrosion debris and high-angle secondary cracks.

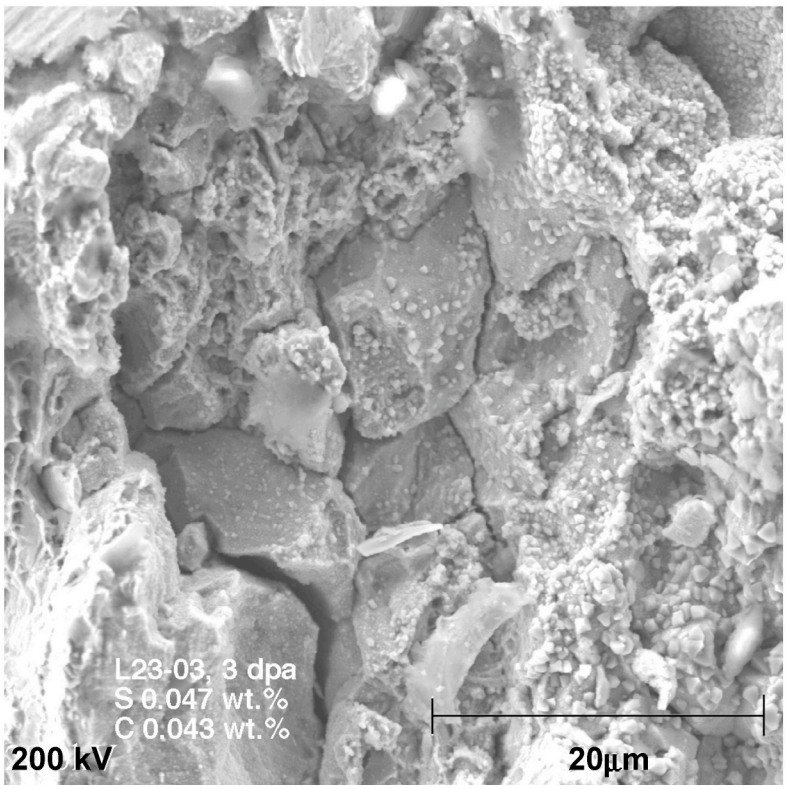

Figure 71. Intergranular fracture surface morphology of IASCC-susceptible Heat L23 (348 SS, 3 dpa). Note corrosion debris and high-angle secondary cracks.

13 Analysis of Grain-Boundary Microchemistry by Auger Electron Spectroscopy

In the consideration of the importance of the roles of S and C in IASCC described in Sections 7-9, the behavior of grain-boundary segregation of the two elements was characterized by Auger electron spectroscopy (AES). Similar analysis by advanced analytical electron microscopy (AAEM) is difficult or impractical for an ordinary grain boundary in an irradiated steel, although S-rich thin films on a crack-tip grain boundary can be detected.[33,34] Auger electron spectroscopy is probably the only practical technique that can characterize well the profile and degree of grain-boundary segregation of S and C in an irradiated steel.

The materials selected for the AES analysis were taken from BWR neutron absorber tubes. The absorber tubes were fabricated from two commercial heats of Type 304 SS (Heats A and B) and were irradiated to 2.0×10^{21} n cm^{-2} ($E > 1$ MeV) (≈3 dpa) during service in a BWR. The behavior of grain-boundary segregation in such material was considered most relevant to BWR IASCC. The neutron absorber tubes were susceptible to field cracking. Unfortunately, neither documented chemical composition of the absorber tubes nor the archive, unirradiated ingots could be found.

Needle-like specimens were prepared from the selected BWR neutron absorber tubes. After cathodically charging with hydrogen at ≈50°C in a solution that contained 100-mg/L $NaAsO_2$ dissolved in 0.1-N H_2SO_4, the needle-like specimen was fractured in a 23°C vacuum in a scanning Auger electron microscope (SAM). In-situ analysis was performed in a JEOL JAMP-10 SAM equipped with automated Ar-sputtering and depth-profiling devices. Four to six ductile fracture surfaces and 12-15 intergranular (IG) fracture surface locations were selected for spot analysis in each specimen. Sulfur and C signals from the selected surfaces were then recorded and compared.

After each spot analysis, a depth-profile analysis was performed on a selected IG fracture surface. The procedure for automated depth-profiling analysis has been described elsewhere.[18,19] Progressive sputtering of the intergranular surfaces with Ar ions and acquisition of the Auger electron signals in the ultra-high vacuum environment of the SAM were controlled by computer.

13.1 Grain-Boundary Segregation of Sulfur and Carbon

An example of an IG fracture surface, produced at 23°C in the H-charged specimens from an absorber tube (304 SS Heat B), is shown in Fig. 72. The IG fracture surfaces reveal numerous deformation steps and a precipitate (diameter ≈15 μm) denoted with number "6". Spots denoted with numbers "5" and "20" were the spots selected for acquisition of Auger electron signals. The results of spot analyses obtained for Tubes A-1 and B are shown in Figs. 73 and 74, respectively. In Fig. 73(a), the peak heights of Auger electrons of S obtained from four ductile fracture surfaces are presented with their counterparts from 12 IG fracture surfaces in Tube A-1. The S intensities from the IG fracture surfaces are significantly higher than their counterparts from ductile-fracture surfaces (i.e., spots not on a grain boundary). This behavior shows that S segregated significantly to grain boundaries (i.e., IG fracture surface) in Tube A-1. Similar results for C are also plotted in Fig. 73(b), which shows that C segregated significantly to grain boundaries in the same tube. Essentially the same behavior was observed for S and C segregation in Tube B; see Fig. 74.

A careful examination of Figs. 73 and 74 reveals that some spots that contain high concentrations of S also contain high concentration of C, e.g., intergranular Spot 16, Tube A-1 and intergranular Spot 12, Tube B. However, whether C segregates preferentially to a grain-boundary region that contains a high concentration of S, or vice versa is not conclusive. This behavior could not be conclusively determined by AES in this investigation; it needs further study by a more direct technique such as field-emission atom-probe technique.

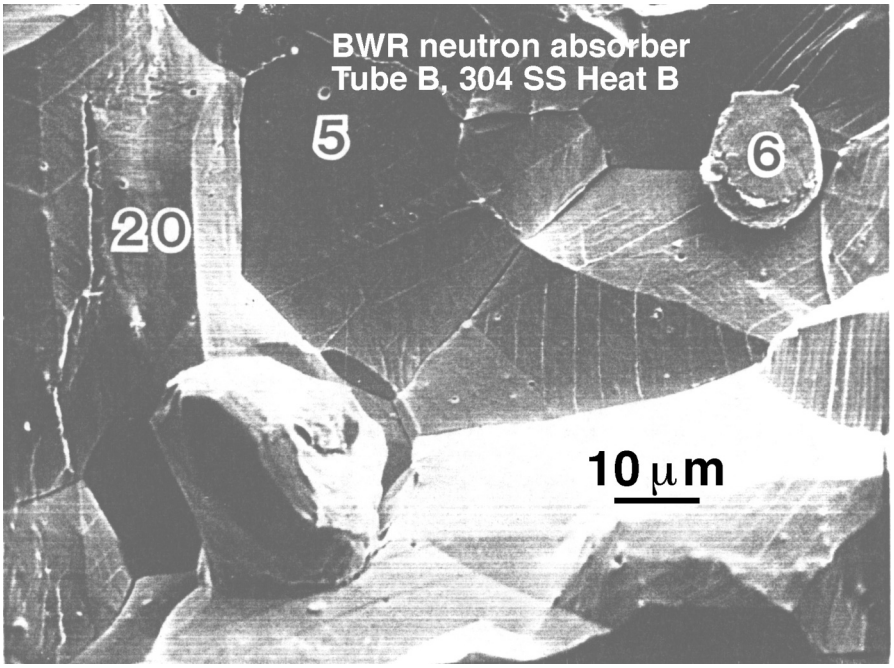

Figure 72. High-magnification fractograph of H-charged BWR neutron absorber tube, 304 SS, Heat B, ≈3 dpa; fracture was produced at 23°C in ultra-high vacuum environment in a scanning Auger electron microscope.

Figure 75 shows the results of depth-profile analysis for the two tubes fabricated from 304 SS Heats A-1 and B. The figure confirms significant grain-boundary segregation of S in Tubes A-1 and B and C segregation in Tube B.

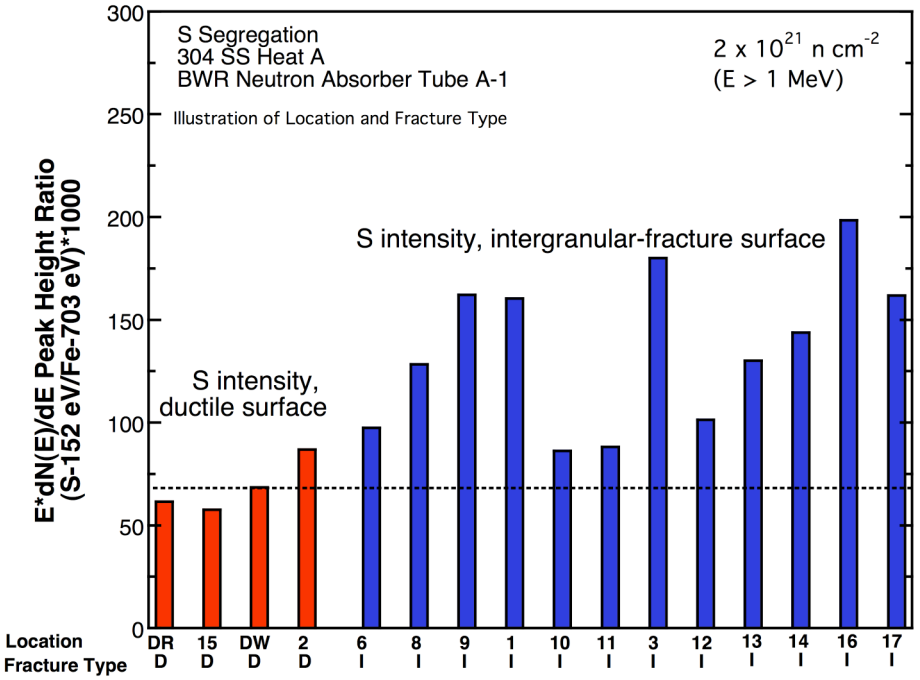

(a)

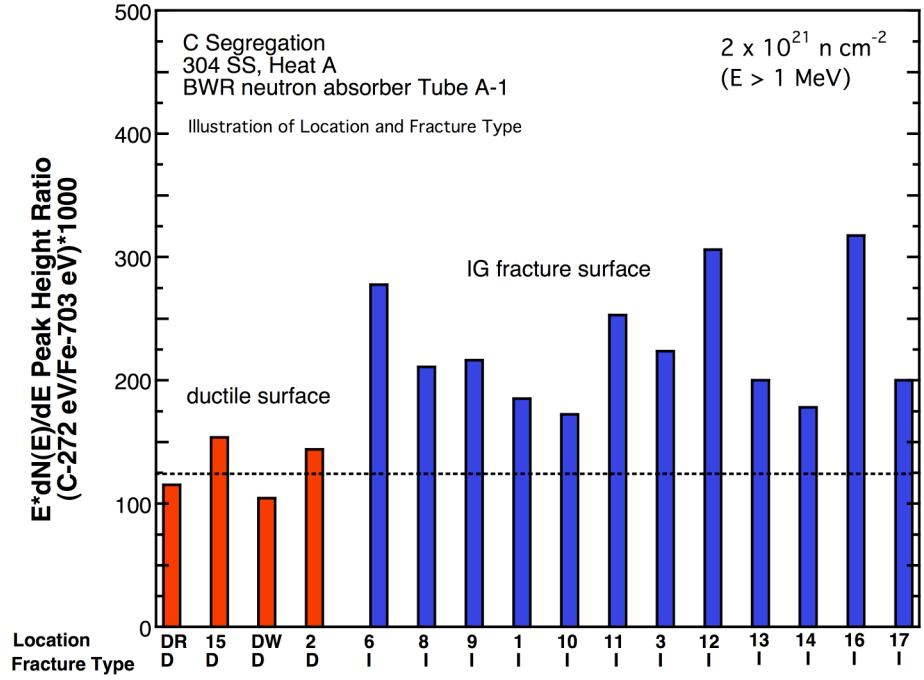

(b)

Figure 73. Summary of AES analysis of grain-boundary segregation of S (a) and C (b) in BWR neutron absorber tube fabricated from Type 304 SS Heat A and irradiated to 3 dpa: S and C peak heights from ductile (denoted “D”) and IG (denoted “I”) fracture surfaces are compared. The horizontal line denotes the average signal strength on a ductile fracture surface.

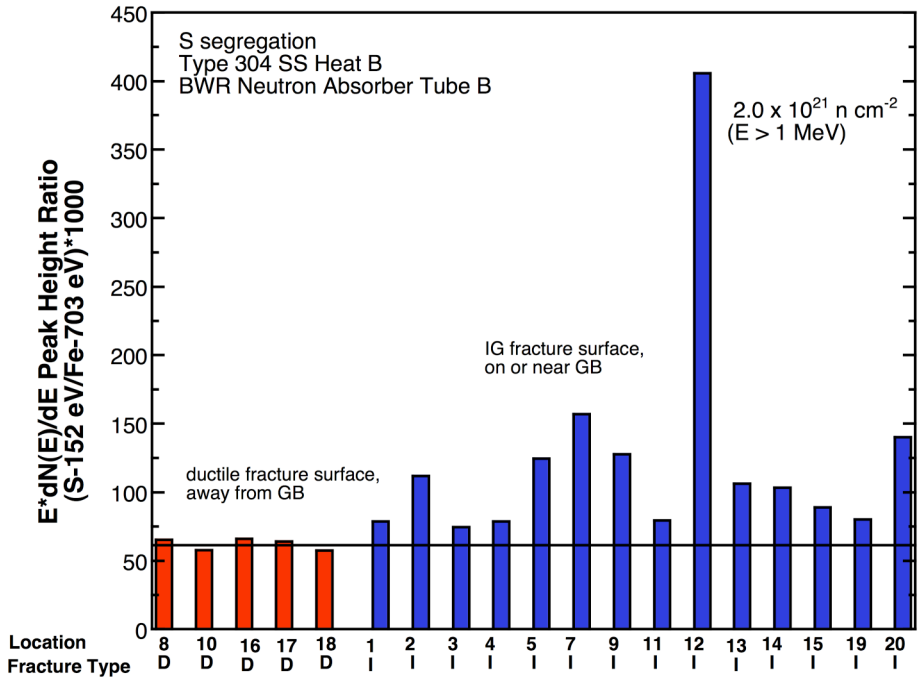

(a)

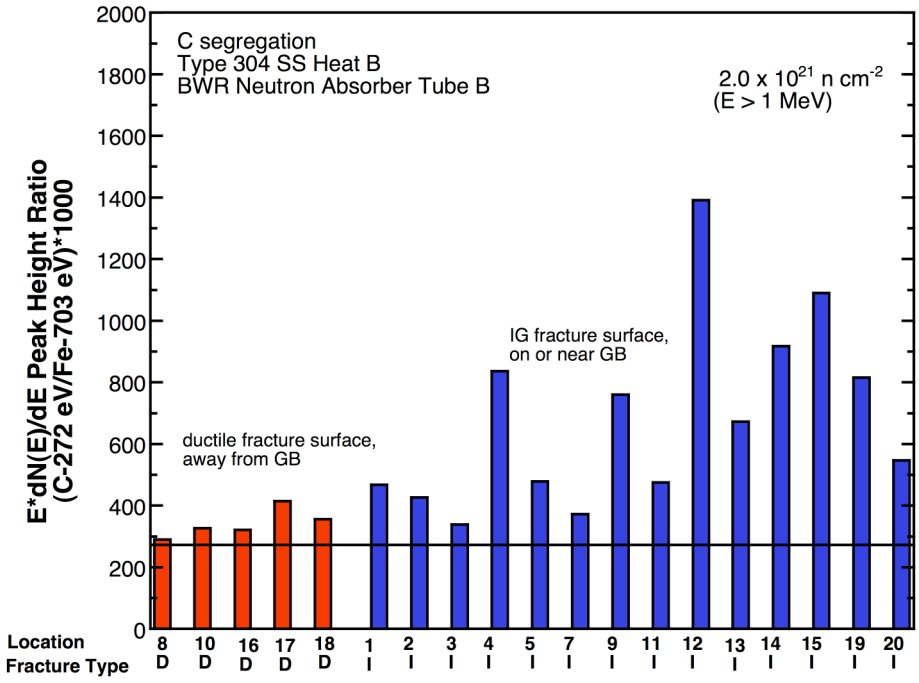

(b)

Figure 74. Summary of AES analysis of grain-boundary segregation of S (a) and C (b) in BWR neutron absorber tube fabricated from Type 304 SS Heat B and irradiated to 3 dpa: S and C peak heights from ductile (denoted “D”) and IG (denoted “I”) fracture surfaces are compared. The horizontal line denotes the average signal strength on a ductile fracture surface.

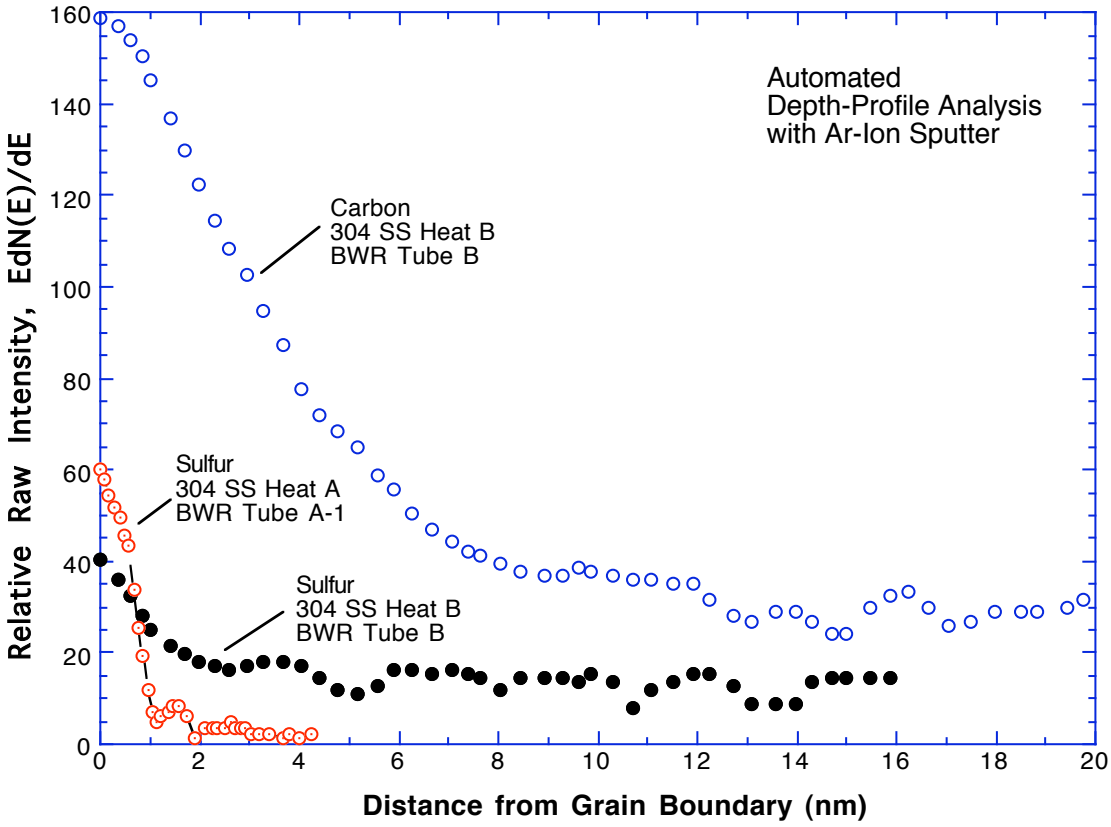

Figure 75. Result of AES depth-profiling analysis of grain-boundary segregation of S and C in BWR neutron absorber tubes fabricated from Type 304 SS Heats A and B and irradiated to ≈3 dpa.

The results in Figs. 73-75, however, do not clarify whether the grain-boundary segregation of S or C occurred via a thermal process (during fabrication), an irradiation-induced process, or both. The former type of segregation is expected to be significantly influenced by several steps during fabrication, e.g., ingot cooling, inter-rolling annealing and cooling, final annealing, and quenching. Thermal segregation is also influenced by plate thickness.

Results of AES analysis of grain-boundary segregation of S have been reported by Jacobs et al.[48] for fuel-cladding-like tubes that were irradiated in a BWR. A tube fabricated from a commercial heat of Type 348 SS was irradiated to 1.5 x 1021 n·cm^{-2} (E > 1 MeV), and a tube fabricated from a high-purity heat of Type 348 SS was irradiated to 3.4 x 10^{21} n·cm^{-2} (E > 1 MeV). Results of spot analysis similar to that of Figs. 73 and 74 showed significant grain-boundary segregation of S in both tubes. Depth-profiling analysis similar to that of Fig. 75 was, however, not reported from their investigation.

Thermal segregation of S to grain boundaries for unirradiated ultra-high-purity (UHP) austenitic SS doped with S has been reported by Andresen and Briant.[49] They concluded that S plays an important role in producing the IG crack path in thermally sensitized non-irradiated steels. Because S atoms are thermally segregated on grain boundaries, more S ions are released into water from the grain boundary than from the grain matrix, and it was thought that an IG crack path is promoted in steels that contain high concentrations of S. Thus, the authors essentially viewed the role of S as accelerating corrosive attack (i.e., dissolution of grain

boundary metal) of a Cr-depleted grain boundary, exacerbated by S ions released into the crack tip water. According to this model, as long as grain boundaries are significantly depleted of Cr, the production of an IGSCC path is predicted, even in a steel free of S.

However, a similar model of the role of S does not appear to explain our results on IASCC susceptibility of irradiated steels. One difficulty is how to explain the observation that IASCC susceptibility becomes negligible when S concentration is very low even though Cr depletion is significant at ≈3 dpa (see Figs. 28 and 43). Another difficulty is how to explain the trend that the S effect is strongly influenced by fluence at >0.003 wt.% S, e.g., in 304- and 316-type steels (see Fig. 29).

13.2 Analysis of Solubility of Carbon in Sulfides

The results in Figs. 42-44 indicate that, when S concentration in a 304- or 316-type steel is ≤0.002 wt.%, a high concentration of C (>0.03 wt.%) promotes a decrease of the susceptibility to IASCC. When S concentration exceeds ≈0.003 wt.%, such a "beneficial" effect of high C concentration appears to be insignificant or absent. This observation suggests that some kind of synergism occurs between S and C and that the effect of such synergism is significant only at sufficiently low concentrations of S (<0.002 wt.%).

With respect to the above observation, our attention was focused on the composition and properties of Ni- and S-rich thin films that were observed on grain boundaries under three situations: i.e., at crack-tip grain boundaries in an unirradiated thermally sensitized crack-growth specimen tested in sulfated BWR-like water (304 SS), reported by Dumbill;[31] at crack-tip grain boundaries in a field-failed BWR top guide and a PWR baffle bolt (304 SS), reported by Thomas and Bruemmer;[33,34] and at ordinary grain boundaries of S-doped Ni specimens that failed during SSRT tests in air at 23°C, reported by Heuer et al.[50] The latter investigators showed that S-doped Ni specimens lose their tensile strength when the grain-boundary concentration of S exceeds ≈15 at.%, which causes an IG failure. Then, it was thought in our study that, if C is dissolved in a Ni_XS_Y-type film in a significant amount, the mechanical properties of such a film are likely to be altered significantly. Accordingly, available information and data were evaluated to determine if C is soluble in sulfides.

The AES signal from the precipitate denoted with number "6" in Fig. 72 is shown in Fig. 76. The AES signal indicates that the precipitate is a CuS-type precipitate that contains a significant amount of C. Similar data are shown in Figs. 77 and 78 for two more CuS-type precipitates that were present in the same specimen.

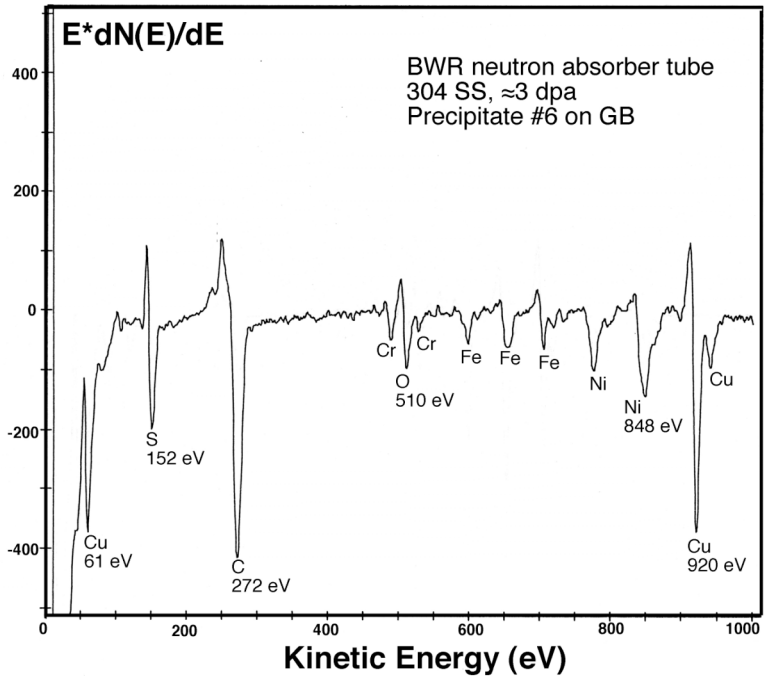

Figure 76.
AES signal showing high concentrations of Cu, S, and C in CuS-type precipitate denoted with number "6" in Fig. 72.

The only direct evidence of significant solubility of C in Ni sulfide could be observed from the data reported by Dumbill.[31] The data (Fig. 6c in his report), obtained by field-emission-gun advanced analytical electron microscopy (FEG-AAEM), show X-ray intensities of Ni, S, and C contained in a Ni- and S-rich thin film that was observed at an intergranular crack in a thermally sensitized, unirradiated Type 304 SS. The FEG-AAEM X-ray spectra strongly indicate that C can be dissolved in significant amounts in Ni- and S-rich thin films at ≈290°C. Unfortunately, similar data were not reported for the field-cracked (irradiated) steels examined by Thomas and Bruemmer.[33,34] However, irradiation is not expected to significantly decrease the solubility of C in the Ni- and S-rich thin films or islands that they observed.

Based on the information described above, it is predicted that C atoms compete with S atoms to become incorporated in the unit cell of NiS-type sulfides under BWR conditions. The degree of such C incorporation, which replaces part of the S atoms in the sulfide, is predicted to be more pronounced for a higher concentration of C at the grain boundary, i.e., for a high C content in the steel and for a higher degree of grain-boundary segregation of C.

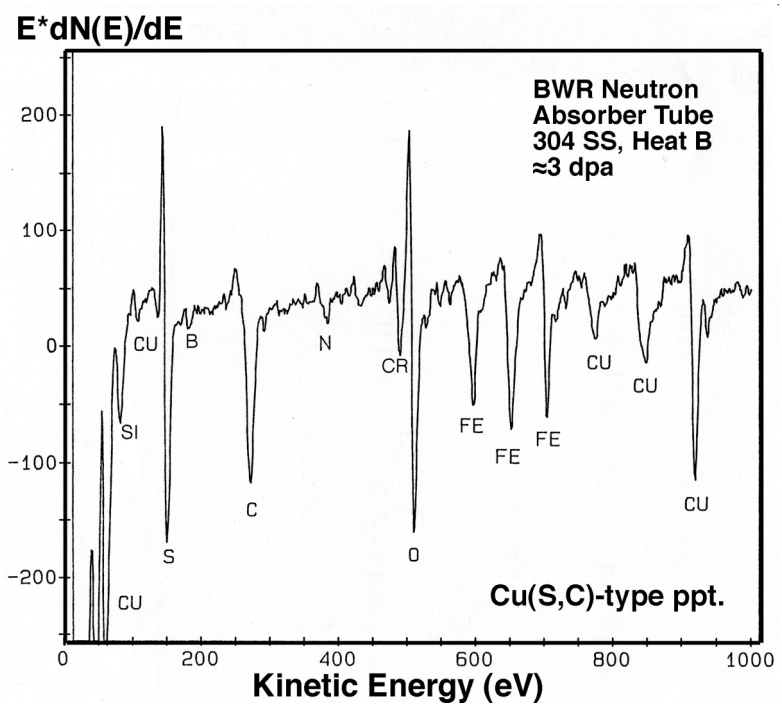

Figure 77.
AES signal showing a high concentration of C in CuS-type precipitate in BWR neutron absorber tube, 304 SS, Heat B, ≈3 dpa.

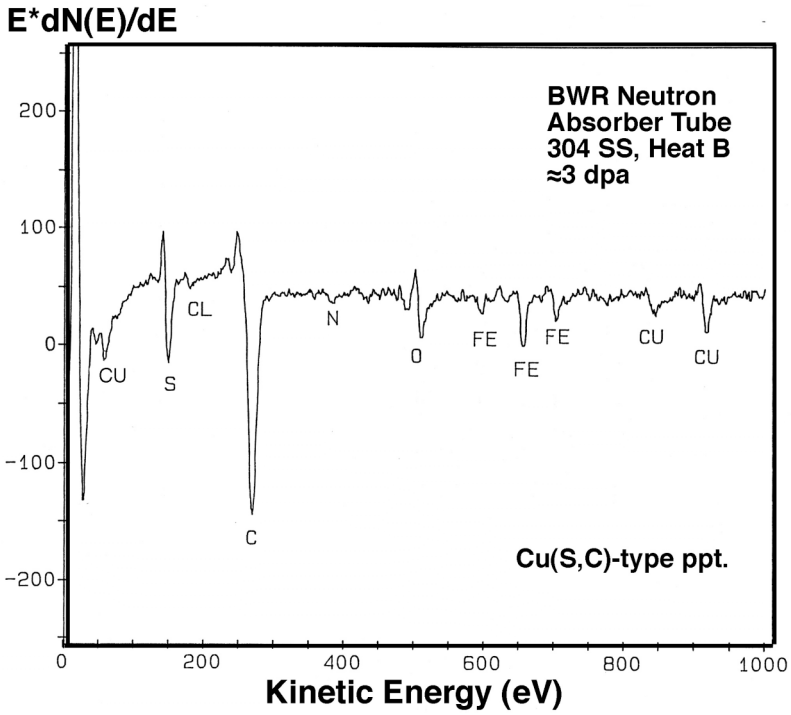

Figure 78.
AES signal showing a high concentration of C in CuS-type precipitate in BWR neutron absorber tube, 304 SS, Heat B, ≈3 dpa.

14 Discussion and Model Development

14.1 General Discussion

The results of this investigation shows that, as neutron fluence increases to a high level (e.g., 2.0 x 10^{21} n cm^{-2} [E > 1 MeV], or 3 dpa), the deleterious effect of S on IASCC susceptibility is dominant over the effects of other elements. The IG fracture surface morphology observed in commercial heats in this study was similar to that of field-cracked BWR core internals. This study also shows that a sufficiently low concentration of S (<0.002 wt.%) is the primary material factor necessary to ensure good resistance to IASCC. Even at slightly higher S concentrations of >0.003 wt.%, Type 304, 304L, 316, and 316L steels were susceptible to IASCC at 3 dpa. This strong dependence on S concentration, shown in Fig. 30 as an example, suggests that some kind of threshold phenomenon related to S is involved in IASCC.

It is important to note that, for 304- and 316-type steels that contain a low concentration of C of <0.03 wt.% (e.g., Types 304L, 316L, and their high-purity counterparts), an S concentration of <0.002 wt.% is not a sufficient material condition to ensure good resistance to IASCC. This behavior is in distinct contrast to the behavior of 304- and 316-type steels that contain high C concentrations of >0.03 wt.% (e.g., Types 304 and 316 steels) and S concentration of <0.002 wt.%. The latter class of steels exhibited good resistance to IASCC. This contrasting behavior indicates that, for S concentration <0.002 wt.%, a high concentration of C plays a beneficial role. However, when S concentration is high, i.e., >0.002 wt.%, it seems that the deleterious effect of S is so pronounced that the effect of a high concentration of C is largely obscured.

At lower damage levels (i.e., <1 dpa), a beneficial effect of a high concentration of Si (i.e., 0.8-1.5 wt.%) was observed. At higher damage levels, however, such effect appears to be obscured by the deleterious effect of S. Therefore, from the standpoint of BWR IASCC, which usually occurs at damage levels >2.5 dpa, we believe that the typical variation in Si concentration in Types 304 and 316 SS (i.e., 0.4 to 1.0 wt.%) is not an important factor. It is not clear if, in addition to a sufficiently low concentration of S (i.e., <0.002 wt.%) and a sufficiently high concentration of C (i.e., >0.03 wt.%), an unusually high concentration of Si (e.g., >1.5 wt.%) provides an extra benefit when fluence is high (e.g., >2.5 dpa). The two heats that belong in this category, i.e., 304 SS Heat L14 (S ≈0.002 wt.%, C 0.107 wt.%, and Si 0.96 wt.%) and 316 SS heat L27 (S ≈0.002 wt.%, C 0.057 wt.%, and Si 1.82 wt.%) exhibited good resistance at 3 dpa. On the other hand, 304 SS Heat C19, which contains a slightly higher S concentration (i.e., 0.003 wt.%) and a relatively low concentration of Si (i.e., 0.45 wt.%), exhibited a significant susceptibility at 3 dpa despite a high concentration of C (i.e., 0.06 wt.%) (see Table 14). Also, 304 SS Heat L6, which contains 0.005 wt.% S and 0.096 wt.% C, exhibited a significant susceptibility at 3 dpa despite a high concentration of Si (i.e., 1.90 wt.%).

Most field-cracked LWR core internals and steels used in SSRT tests or to evaluate crack-growth behavior in the IASCC community contain S concentrations >0.002 wt.%. Therefore, it is not surprising to see that most of them were susceptible to IASCC in one way or another. For S concentrations >0.002 wt.%, the degree of IASCC susceptibility in this study varied significantly from heat to heat, and it was difficult to predict the degree quantitatively. This behavior, consistent with literature data, is not unexpected when one considers the fact that, for a given fluence level, several factors can influence the degree of S segregation to grain boundaries, e.g., annealing and cooling history during fabrication, Mn content, precipitation of sulfides such as MnS and CuS, and solubility of the sulfides in BWR-like water.

The observation that steels that contain a very low or negligible amount of S are resistant to IASCC provides an important clue to the mechanism of IASCC. To understand the mechanism, we believe it is important to consider the following:

(1) The strong dependence of IASCC susceptibility on fluence

(2) The strong dependence of IASCC susceptibility on S concentration and an indication that some kind of critical phenomenon involving S occurs

(3) A high concentration of C (>0.03 wt.%) suppresses IASCC susceptibility at sufficiently low S concentrations (<0.002 wt.%) but not at S concentrations >0.003 wt.%.

(4) Very low solubility of S in an austenitic SS at ≈300°C

(5) Segregation of S to grain boundary

(6) Parallel grain-boundary Cr depletion and Ni segregation

(7) Strong influence of water chemistry on BWR IASCC

(8) Strong effect of strain rate on percent IGSCC from SSRT tests

Considering the finding that the S effect is dominant at high fluence and the fact that grain-boundary Cr depletion is in some respect a mirror image of grain-boundary Ni segregation, we believe it is important to understand the peculiar properties of Ni-S thin film reported by Heuer et al., who investigated the effect of ion-implanted S on disorder-induced amorphization of Ni.[50] Those authors also investigated the effect of thermal segregation of S on grain boundaries on the mechanical properties of unirradiated binary Ni-S. In the latter investigation, they found that, as the grain boundary concentration of S exceeds ≈10 at.% (≈5.6 wt.%), the mechanical properties of S-segregated Ni start to degrade drastically in 23°C air, i.e., there is a precipitous decrease in total elongation, tensile strength, modulus of toughness, reduction-in-area, and a sharp increase in percent intergranular cracking (IGC). This means that, at a sufficiently high level of S segregation, a grain boundary in the Ni-S system loses metallic strength and behaves more like a clay. Okamoto and his coworkers also showed that the volume fraction of amorphization of S-ion-implanted specimens starts to increase drastically when the bulk S concentration exceeds ≈5.6 wt.%.[50,51] Based on these observations, they concluded that S-induced intergranular fracture in binary Ni-S is explained well by disorder-induced melting of a Ni-S-rich thin film that formed on grain boundaries. They proposed that this process is strongly influenced by S and H concentrations, stress, temperature, and irradiation damage. We believe that the results of Okamoto and his coworkers constitute a very useful framework that can shed light on the mechanistic understanding of IASCC.

Similar to the observation of Heuer et al.,[50] predominantly IG fracture was observed in one of our high-strain-rate bending tests in 23°C air, specifically, a Type 304 SS Heat L13, which contained an unusually high concentration of S (0.022 wt.%) and an unusually low concentration of Mn (0.36 wt.%). The specimen was neither exposed to water nor charged with hydrogen before the bending test. Therefore, the intergranular fracture in the specimen cannot be explained on the basis of H-induced embrittlement of grain boundaries. The high-magnification intergranular fractograph of the specimen, shown in Fig. 79, is characterized by a

smooth grain boundary separation, a virtual absence of deformation steps, and an indication of significant grain encirclement. These features are similar to those of IASCC failures produced in 289°C water. Because the specimen was irradiated in high-purity helium, it is also difficult to explain the intergranular fracture by grain boundary oxidation or O segregation. The fracture behavior seems to differ from limited amount of near-surface intergranular separation reported by Onchi and his coworker[52,53] for thermally sensitized and irradiated 304 SSs that were tested in inert gas at ≈290°C. Nevertheless, the experiment of Fig. 79 shows that purely mechanical intergranular failure similar to that reported in the unirradiated Ni-S system can occur in a highly irradiated austenitic SS that contains an unusually high concentration of S.

Considering the observations discussed above, we believe that it is important to better understand the structure and properties of Ni- and S-rich thin films and islands that have been reported by Thomas and Bruemmer[32-34] and Dumbill.[31] The former investigators conducted extensive studies on crack-tip microstructure and microchemistry of field-cracked BWR and PWR core internal components.[33,34] Similar studies were also performed by Dumbill[31] and Bruemmer and Thomas[32] on unirradiated, thermally sensitized 304[31] and 316[32] SSs that were tested in sulfated[31] or deoxygenated[32] BWR-like water at 289°C.

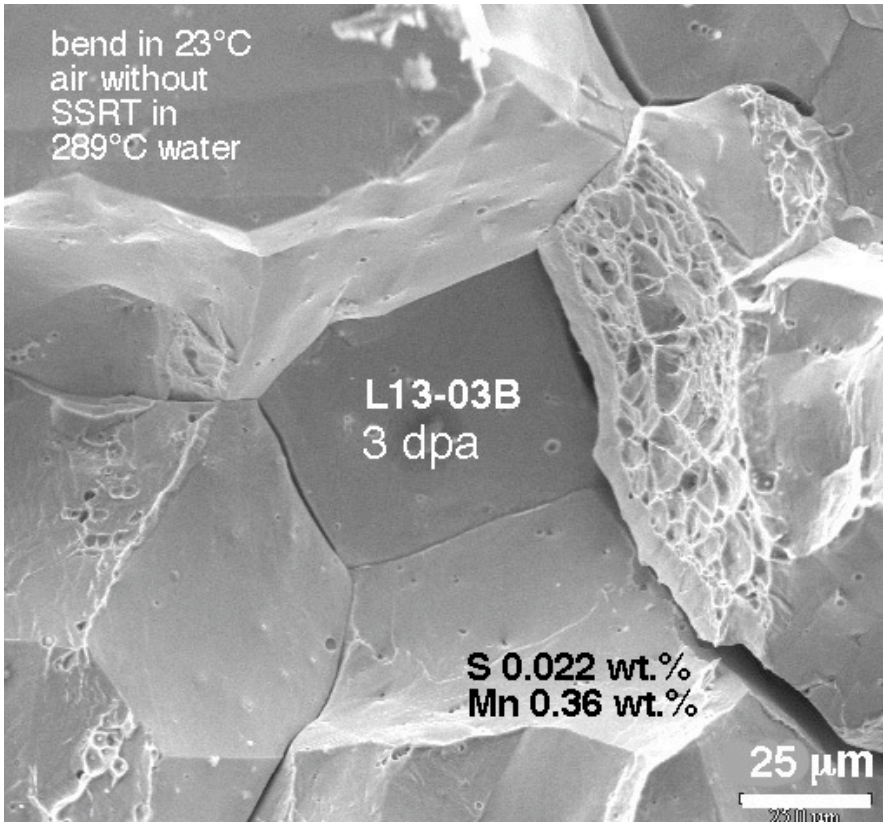

Figure 79. Fracture surface morphology of high-S, low-Mn Type 304 SS Specimen L13-03B (S, 0.022 wt.%; Mn, 0.36 wt.%; ≈3 dpa in helium at 289°C) produced during bending in 23°C air without previous exposure to water or H charging.

In Ref. 33, Thomas and Bruemmer report extensively on the crack-tip grain boundary microstructural characteristics of a PWR baffle bolt and a BWR top guide, both of which cracked during service. A layer of

Cr-Fe-type spinel oxide sandwiched between the two adjacent grain matrices was always observed ahead of an open crack tip. Such an oxide was fine-grained and contained tiny pores (diameter 2-10 nm). In the case of the BWR top guide, numerous irregularly shaped microcavities, as large as ≈100 nm in length and ≈50 nm in width, were observed, usually at the metal/oxide boundary and near the tip of the spinel oxide.

Direct evidence of Ni_xS_y-type thin films produced between such a spinel oxide and the metal matrix is observed in several photomicrographs, e.g., Figs. 3-10 and 3-13 in Ref. 33 for the PWR baffle bolt. Small islands of Ni or Ni_xS_y-type phase are also observed. The width of such Ni_xS_y-type thin film is extremely small, i.e., <7 nm, based on data from energy-dispersive spectroscopy (EDS) and <3 nm based on bright-field image. In the case of the BWR top guide, a similar type of thin film (thickness ≈3 nm), which exhibits the same imaging contrast is observed at the boundary between the metal matrix and the spinel oxide, e.g., Figs. 4-11, 4-12, 4-14, 4-17, and 4-20 of Ref. 33.

Results of analysis by energy dispersive spectroscopy on the top guide indicate that such film contains a high concentration of Ni. However, data for S distribution near the film were not reported. The distance between EDS spots in the analysis was 5-25 nm, significantly larger than the width of such a thin film. Under such conditions, one can easily miss probing a spot correctly placed in the middle of a thin film that is only <3 nm wide. Therefore, it is not easy to measure the distribution of S near such a film. However, microstructural features such as spinel oxide, voids, cavities, the position and shape of an open crack, and Ni_xS_y-type thin film can be detected readily through bright-field imaging and tilting. A dark-field image of a <3-nm-wide Ni_xS_y-type thin film, which is a more valuable piece of information, would be very difficult to obtain in an irradiated core internal. Dumbill reported results of X-ray mapping that show a matching distribution of Ni and S for a crack tip in his unirradiated sensitized 304 SS specimen.[31] The Ni- and S-rich thin film in his specimen was relatively thicker (i.e., width ≈100 nm), and a continuous EDS line scan and matching elemental mapping that clearly showed the nature of such film could be obtained.

Thomas and Bruemmer provided a comprehensive interpretation of the crack-tip microstructures observed in their studies.[33,34] They suggested that Cr- and Fe-rich spinel oxide, observed ahead of an open crack tip, was produced as a corrosion byproduct that filled the crack opening after the crack had advanced along the grain boundary. Thus, the spinel oxide tip was interpreted to be the same as the crack tip. Formation of Ni-rich thin films and islands was attributed to a mechanism of selective dissolution in which Cr and Fe atoms are dissolved preferentially over Ni atoms in the crack-tip water.

Nevertheless, photomicrographs and EDS data given in the reports of Thomas and Bruemmer[32-34] or Dumbill[31] shed light on several new clues that are helpful to the understanding of the metallurgical processes that occur near a crack tip. Thus, we thought that a more detailed integrated evaluation is timely. Several important observations in the following discussion suggest a mechanism in which spinel oxide and Ni and Ni_xS_y thin films and islands visible near the crack tip were produced, not after the crack advanced to the position of the spinel oxide tip, but, instead, before the crack advanced in association with internal grain-boundary oxidation which occurred ahead of the crack tip.

The first observation is that a crack tip is often visible adjacent to a grain boundary rather than in line with the grain boundary. The offset distance between the line of crack advance and the grain boundary (imaged edge on) was ≈20 nm in the field-cracked BWR top guide; see Figs. 4-19 and 4-21 in Ref. 33. In the case of unirradiated thermally sensitized 304 and 316 SSs tested in deoxygenated BWR-like water, the offset distance was ≈90 nm and ≈15 nm, respectively, (Ref. 32). This observation is difficult to explain on the basis

of preferential dissolution of the grain-boundary metal; it is equally difficult to explain on the basis of a premise that the grain boundary itself shifts continuously ahead of an advancing crack tip. The offset distance is, in fact, the same as the distance between the grain boundary and the metal/spinel boundary, in which a Ni_xS_y-type thin film and islands are present, often accompanied by high-density voids and cavities. More voids and cavities tend to appear in regions where thin films or islands of Ni_xS_y-type or Ni-rich phases occur. This observation suggests that the voids and cavities were products of localized melting of Ni- and S-rich films or islands. This view is essentially consistent with the results of experiments and the theory advanced by Okamoto and his coworkers on the behavior of S-rich thin film in the Ni-S binary system.[50,51]

The second observation is dark-field morphology of spinel oxide present ahead of an open crack tip. Such a dark-field image was reported in Ref. 32 for a crack tip in an unirradiated, thermally sensitized 316 SS. In the image, extremely small particles of spinel oxide (diameter ≈5 nm) are observed decorating the grain boundary ≈290 to ≈450 nm ahead of the open crack tip, and twin boundaries ≈350 nm ahead of the crack tip. This observation provides direct evidence of internal oxidation on grain boundaries and twin boundaries in a BWR-like environment, and it is reasonable to expect a similar phenomenon in a BWR core internal. For ordinary grain boundaries (i.e., grain boundaries that are not involved in crack-tip advancement), evidence of grain-boundary internal oxidation has been reported only for the heat-affected zone (HAZ) in BWR core shroud welds that were prepared by shielded-metal-arc or submerged-arc procedure.[26,54] Oxygen contamination in such a HAZ is pronounced, and because O solubility in the grain matrices is extremely low near room temperature, O atoms segregate to grain boundaries during cooling of the HAZ. Internal oxide particles produced by this process have been characterized by Auger electron spectroscopy in Refs. 26 and 54 by transmission electron microscopy in Ref. 26.

The third observation is pores and voids that decorate previous twin boundaries located within a spinel oxide ahead of an open crack tip. Such a feature, visible in a top guide crack tip in Figs. 4-9 and 4-10 of Ref. 33, cannot be explained on the basis of a premise that the spinel oxide filled the crack opening up to the tip of the spinel oxide. Such a feature is, however, explained well based on a premise that a grain boundary region that contains a twin was oxidized internally before the crack advanced to that particular location.

The fourth observation notes the tendency that more cavities are observed near the tip of the spinel oxide layer than near the metal/spinel boundary, e.g., the top guide crack-tip structure shown in Figs. 4-20 to 4-25 of Ref. 33. Also, more Ni and Ni-sulfide islands tend to be present near the tip of a spinel oxide, e.g., Figs. 3-14 (baffle bolt) and 4-18 (top guide) in Ref. 33. This behavior is not explained well based on a premise that the spinel oxide filled the crack opening but is explained well based on a premise that the spinel oxide extended its length via internal oxidation of the grain-boundary. In the latter process, Cr and Fe atoms are expected to be selectively oxidized by the oxygen atoms that diffuse down the grain boundary, thereby gradually enriching the metal near the tip of the oxide with Ni. At the same time, S atoms are predicted to remain in the metal ahead of the spinel tip rather than being incorporated in the spinel oxide in which their solubility is lower (than in the metal).

The above observations lend strong support to a mechanism in which a spinel oxide layer and Ni- and S-rich thin films and islands are produced ahead of an advancing crack tip, and localized melting of the Ni- and S-rich films and islands plays a primary role in crack propagation. The result of such melting is the production of voids and cavities at the metal/spinel boundary and near the tip of the spinel layer.

14.2 An IASCC Model

On the basis of several key observations in this study and elsewhere, and on the basis of the discussions above, we propose a new IASCC mechanism for irradiated austenitic SS. The model, initially reported in Ref. 55 and schematically illustrated in Fig. 80, is based on the following steps, some postulated and some supported by observations in this study or other investigations:

(1) Many incipient cracks are nucleated in the brittle surface oxide layer that is in contact with water.

(2) When one such incipient crack encounters a grain boundary, the metal in front of the crack tip is oxidized preferentially along the grain boundary, because stress and defects (crystallographic and irradiation-induced defects) are higher at the grain boundary. A grain boundary is a preferential path for faster diffusion of O from the water, especially in a highly irradiated steel.

(3) The rate of O transport from water to grain-boundary metal is strongly influenced by the thickness and morphology of the Cr oxide layer that covers the crack-tip grain boundary. When grain boundary Cr depletion is significant, the Cr oxide layer is thinner and less protective, which allows a faster permeation and transport of O. If the Cr oxide layer that covers the crack-tip grain boundary is ruptured by twinning or dislocation channeling, O transport to the grain-boundary metal is facilitated.

(4) The metal at the crack-tip grain boundary is gradually converted to Cr-Fe-type spinel oxide, because Cr and Fe atoms are preferentially (or selectively) oxidized over Ni atoms by the O atoms that diffused down the grain boundary. Nickel atoms are significantly more difficult to oxidize than Fe and Cr. The free energies of oxidation at ≈300°C of Ni, Fe, and Cr are, respectively, –92, –111, and –155 kcal/mole of O_2. Thus, most Ni atoms remain unoxidized in the metal matrix. The result is that, Ni atoms, excluded from the growing Cr-Fe spinel oxide layer on the grain boundary, accumulate near the metal/spinel boundary and at the tip of the spinel oxide.

(5) At the same time, S atoms segregated on the grain boundary are also pushed out of the spinel oxide, because the solubility of S is lower in the oxide than in the metal.

(6) Eventually, Ni- and S-rich thin films or islands form at the metal/spinel boundary and at the tip of the growing spinel oxide layer. The Ni- and S-rich region can be in the shape of a continuous or discontinuous film or a small isolated island. Nickel and S atoms accumulate more at the tip of the long spinel oxide layer than at the metal/spinel boundary, because less oxidation occurs in the latter direction.

(7) Some S ions accumulate in the crack tip water because of dissolution of soluble sulfides.[56] Some S atoms are released into the metal due to irradiation-induced instability of MnS[57] and subsequently diffuse to the thin region of metal that is in contact with the Ni- and S-rich film under the influence of high tensile stress.

(8) When the concentration of S in the Ni- and S-rich thin film or island exceeds a threshold level, the film or island melts or is amorphized, thereby losing its metallic strength. When the thin film or island melts, voids and cavities are formed near the metal/spinel boundary and at the tip of the spinel layer.

(9) The crack tip then advances along the weakened metal/oxide boundary, i.e., along the thin region in which the Ni- and S-rich thin film and islands melt or are amorphized, thereby producing voids and cavities.

(10) Voids and cavities tend to be produced more ahead of the spinel tip than at the metal/spinel boundary because of the factor described in Step 6. When a large cavity(ies) form at the spinel tip, crack advance halts until a new spinel layer forms ahead of such a cavity(ies). At this time the line of crack advance can switch.

(11) Once the Ni- and S-rich thin films or islands melt or are amorphized, they lose their crystalline structure. The polyhedral crystal structure of the phase, such as the cage structure described by Ashby and Spaegen,[58] is broken. Then, the S atoms incorporated in the polyhedral cages diffuse away into the metal matrix.

(12) Depending on postcracking thermal history, the degree of such back-diffusion of S atoms varies. Then, the S-to-Ni ratio and the distribution of S and Ni near voids and cavities observed in a post-cracking examination may vary significantly.

14.3 Role of Carbon

The role of carbon that tends to suppress IASCC susceptibility at very low concentrations of S (≤0.002 wt.%) is not well understood at this time. However, an attractive model that can explain the beneficial effect is based on a postulation that C atoms are dissolved in significant amounts in the Ni- and S-rich thin film. As shown by Heuer et al. a Ni- and S-rich thin film loses metallic strength when the S content in the film exceeds a threshold level.[50] Such a loss of metallic strength is attributed to severe localization of free electrons by S atoms incorporated in the Ni-S-type film, i.e., trapping of free electrons by S. When deprived of free electrons, the film no longer exhibits metallic behavior or metallic strength. A simple consideration suggests that C atoms can easily occupy the same octahedral sites in the unit cell of Ni sulfide that would be normally occupied by S atoms. Thus, when C concentration is high near the Ni- and S-rich thin film that is formed at the crack-tip grain boundary, S and C atoms compete to occupy the same octahedral sites. Under such a situation, C dissolved in the film is expected to promote a strong covalent bonding with Ni, in effect suppressing the effect of trapping free electrons by S. The limited information described in Section 13.2 indicates that the solubility of C in a CuS- and NiS-type thin film is significant, which is consistent with, but does not prove, the model outlined above. A further investigation is desirable to provide a better mechanistic understanding of the role of C atoms on BWR IASCC.

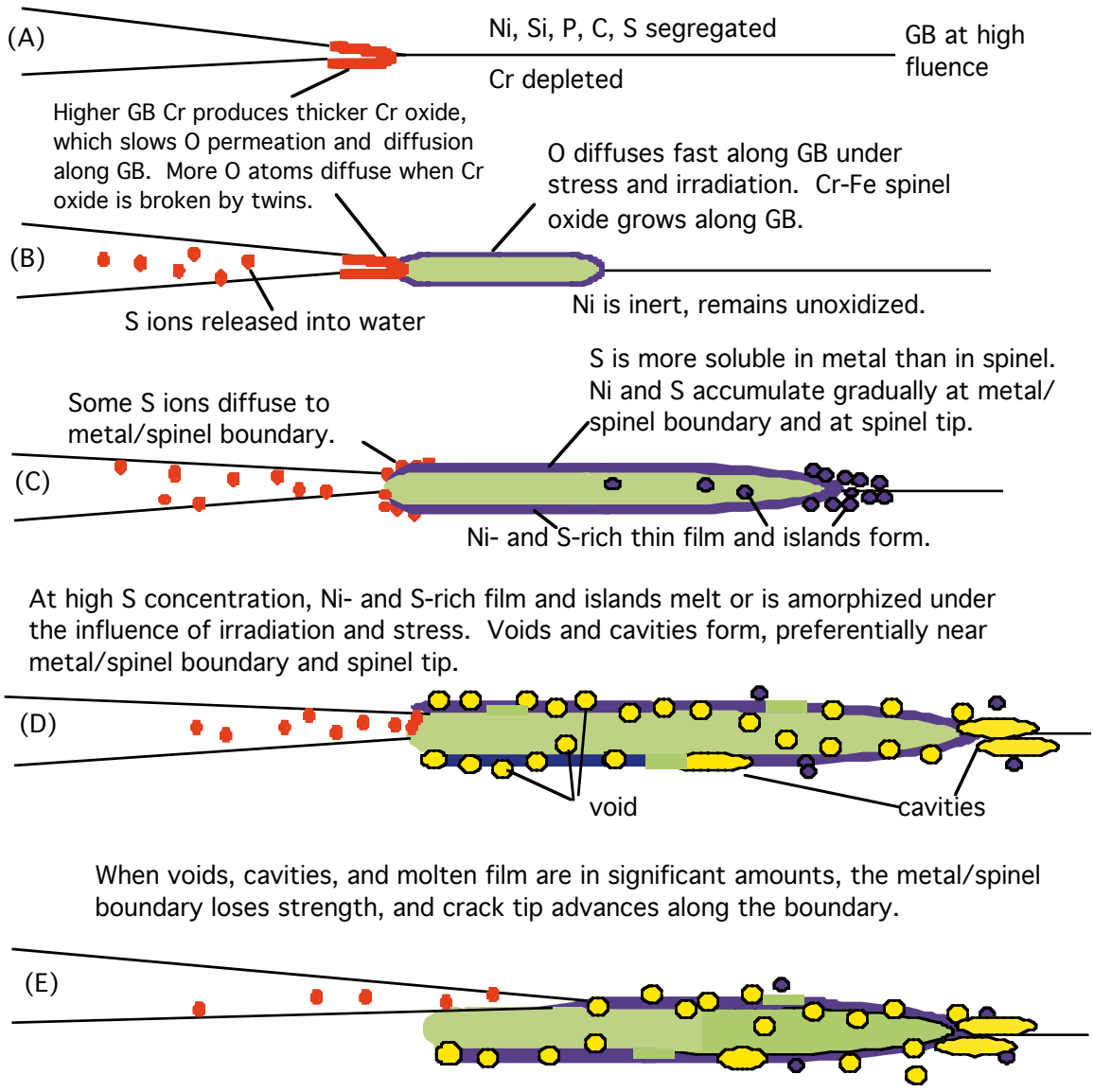

Figure 80. Schematic illustration of an IASCC model

15 Conclusions

Slow-strain-rate tensile tests in BWR-like water (dissolved oxygen ≈8 ppm) and fractographic analysis were conducted on commercial and laboratory-fabricated model heats of austenitic stainless steels irradiated at 289°C in helium to ≈0.3 x 10^{21} n cm^{-2}, ≈0.9 x 10^{21} n cm^{-2}, and ≈2.0 x 10^{21} n cm^{-2} (E > 1 MeV) (≈0.4, 1.4, and ≈3 dpa). Susceptibility of the steels to irradiation-assisted stress corrosion cracking (IASCC) was determined on the basis of the degree of intergranular fracture surface morphology. The investigation has led to the following conclusions.

(1) At ≈0.4 dpa, IASCC susceptibility was negligible for all tested heats, with the exception of a 316L-like high-purity alloy that contained 0.003 wt.% C and 0.004 wt.% S. At 0.4 and 1.4 dpa, significant transgranular fracture was mixed with intergranular fracture. At 3 dpa, the tendency to transgranular stress corrosion cracking was negligible, and fracture surface morphology was either dominantly intergranular, as in field-cracked core internal components, or dominantly ductile or mixed. This behavior indicates that percent IGSCC determined at ≈3 dpa is a good measure of IASCC susceptibility.

(2) At 1.4 dpa, a beneficial effect of a high concentration of Si (0.8-1.5 wt.%) was observed. At 3 dpa, however, such effect was obscured by a strongly deleterious effect of S. From the standpoint of BWR IASCC, which usually occurs at >2.5 dpa, typical variation in Si concentration in the range of 0.4-1.1 wt.% in Types 304, 316, and 348 steel is, therefore, not an important factor.

(3) Excellent resistance to IASCC was observed up to ≈3 dpa for seven heats of Types 304 and 316 steel that contain very low S concentrations of ≤0.002 wt.% and for one heat of Type 348 steel that contains 0.005 wt.% S. Susceptibility of Types 304 and 316 steel that contain >0.003 wt.% S increased drastically. These observations indicate that a sulfur-related critical phenomenon plays an important role in IASCC. A sufficiently low concentration of S (i.e., <0.002 wt.%) is the primary material factor necessary to ensure good resistance to IASCC.

(4) For Types 304L and 316L steel and their high-purity counterparts that contain <0.025 wt.% C, a sulfur concentration of <0.002 wt.% alone is not a sufficient material condition to ensure good resistance to IASCC. This is in distinct contrast to the behavior of the high-C counterparts (i.e., Types 304 and 316 steel that contain <0.002 wt.% S and >0.03 wt.% C), which exhibit good resistance to IASCC. The contrasting behavior indicates that, at sufficiently low concentrations of S, a high concentration of C is beneficial. However, at S concentrations >0.003 wt.%, the deleterious effect of S is so dominant that a high concentration of C is not an important factor.

(5) A two-dimensional map was developed in which susceptibility or resistance to IASCC is shown as a function of bulk concentrations of S and C. Data reported in the literature are consistent with the map. The map is helpful to predict relative IASCC susceptibility of Types 304 and 316 steel. A similar map is helpful to predict IASCC behavior of Type 348 steel.

(6) At S concentrations >0.003 wt.%, IASCC susceptibility is thought to be influenced significantly by various material-related factors, such as the degree of S segregation to grain boundaries, annealing and cooling during fabrication, component thickness, presence of delta ferrite, Mn content, precipitation of

sulfides, solubility of sulfides in the crack-tip water, and the thickness and morphology of the Cr oxide on the crack-tip grain boundary, which controls oxygen permeation and diffusion along the grain boundary.

(7) A model alloy that contains ≈3 vol.% globular-shaped delta ferrite and ≈21 wt.% Cr exhibited excellent resistance to IASCC, despite the fact that it contained a very high S concentration of 0.028 wt.%. The excellent resistance is attributed to the effect of delta ferrite, which traps S atoms, and the effect of a high concentration of Cr, which forms Cr oxide and helps to block oxygen permeation and diffusion along the austenite grain boundary.

(8) Grain-boundary segregation of S was observed for BWR neutron absorber tubes. It is not clear, however, whether the S segregation occurred via a thermal process, an irradiation-induced process, or both.

(9) Based on the results of this study, an IASCC model has been developed. The model is based on several key steps known or postulated to occur at the crack-tip grain boundary, i.e., grain-boundary segregation of Ni and S, preferential oxidation of Cr and Fe atoms over Ni atoms by oxygen that diffuses along the grain boundary, formation of a Cr-Fe spinel oxide ahead of the crack tip, formation of Ni- and S-rich thin films and islands at the metal/spinel boundary, and melting or amorphization of the Ni-and S-rich thin films and islands. The model also predicts that the thickness and morphology of the Cr oxide that covers the crack-tip grain boundary strongly influence the rate of oxygen permeation and diffusion along the grain boundary.

References

1. A. J. Jacobs, G. P. Wozadlo, K. Nakata, T. Yoshida, and I. Masaoka, "Radiation Effects on the Stress Corrosion and Other Selected Properties of Type-304 and Type-316 Stainless Steels," in Proc. 3rd Intl. Symp. Environmental Degradation of Materials in Nuclear Power Systems – Water Reactors, August 30-September 3, 1987, Traverse City, MI, G. J. Theus and J. R. Weeks, eds., The Metallurgical Society, Warrendale, PA, 1988, pp. 673-680.

2. F. Garzarolli, D. Alter, P. Dewes, and J. L. Nelson, "Deformability of Austenitic Stainless Steels and Ni-Base Alloys in the Core of a Boiling and a Pressurized Reactor," in Proc. 3rd Intl. Symp. Environmental Degradation of Materials in Nuclear Power Systems – Water Reactors, August 30-September 3, 1987, Traverse City, MI, G. J. Theus and J. R. Weeks, eds., The Metallurgical Society, Warrendale, PA, 1988, pp. 657-664.

3. K. Fukuya, K. Nakata, and A. Horie, "An IASCC Study Using High Energy Ion Irradiation," in Proc. 5th Intl. Symp. on Environmental Degradation of Materials in Nuclear Power Systems – Water Reactors, August 25-29, 1991, Monterey, CA, D. Cubicciotti, E. P. Simonen, and R. Gold, eds., American Nuclear Society, La Grange Park, IL, 1992, 814–820.

4. M. E. Indig, J. L. Nelson, and G. P. Wozadlo, "Investigation of Protection Potential against IASCC," in Proc. 5th Intl. Symp. on Environmental Degradation of Materials in Nuclear Power Systems – Water Reactors, August 25-29, 1991, Monterey, CA, D. Cubicciotti, E. P. Simonen, and R. Gold, eds., American Nuclear Society, La Grange Park, IL, 1992, pp. 941-947.

5. M. Kodama, S. Nishimura, J. Morisawa, S. Shima, S. Suzuki, and M. Yamamoto, "Effects of Fluence and Dissolved Oxygen on IASCC in Austenitic Stainless Steels," in Proc. 5th Intl. Symp. on Environmental Degradation of Materials in Nuclear Power Systems – Water Reactors, August 25-29, 1991, Monterey, CA, D. Cubicciotti, E. P. Simonen, and R. Gold, eds., American Nuclear Society, La Grange Park, IL, 1992, pp. 948-954.

6. H. M. Chung, W. E. Ruther, J. E. Sanecki, A. G. Hins, and T. F. Kassner, "Effects of Water Chemistry on Intergranular Cracking of Irradiated Austenitic Stainless Steels," in Proc. 7th Int. Symp. on Environmental Degradation of Materials in Nuclear Power Systems - Water Reactors, August 7-10, 1995, Breckenridge, CO, G. Airey et al., eds., NACE International, Houston, 1995, pp. 1133-1143.

7. F. Garzarolli, P. Dewes, R. Hahn, and J. L. Nelson, "Deformability of High-Purity Stainless Steels and Ni-Base Alloys in the Core of a PWR," in Proc. 6th Intl. Symp. on Environmental Degradation of Materials in Nuclear Power Systems - Water Reactors, August 1-5, 1993, San Diego, CA, R. E. Gold and E. P. Simonen, eds., The Minerals, Metals, and Materials Society, Warrendale, PA, 1993, pp. 607-613.

8. I. Suzuki, M. Koyama, H. Kanasaki, M. Akiyama, T. Okubo, Y. Mishima, and T. R. Mager, "Stress Corrosion Cracking of Irradiated Stainless Steels in Simulated PWR Primary Water," in Proc. 4th Intl. Conf. on Nuclear Engineering, 1996, Vol. 5, p. 205, American Society of Mechanical Engineers, New York.

9. H. Kanasaki, T. Okubo, I. Satoh, M. Koyama, T. R. Mager, and R. G. Lott, "Fatigue and Stress Corrosion Cracking Behavior of Irradiated Stainless Steels in PWR Primary Water," in Proc. 5th Intl. Conf. on Nuclear Engineering, March 26-30, 1997, Nice, France.

10. J. Coneman, R. P. Shogan, D. R. Forsyth, I. L. W. Wilson, and H.-T. Tang, "Characterization of Baffle Former Bolts Removed from Service in US PWRs," in CD, Proc. 10th Intl. Conf. on Environmental Degradation of Materials in Nuclear Power Systems - Water Reactors, Aug. 5-9, 2001, Lake Tahoe, Nevada.

11. R. P. Shogan and T. R. Mager, "Susceptibility of Type 316 Stainless Steel to Irradiation-Assisted Stress Corrosion Cracking in a PWR Environment," in CD, Proc. 10th Intl. Conf. on Environmental Degradation of Materials in Nuclear Power Systems - Water Reactors, Aug. 5-9, 2001, Lake Tahoe, Nevada.

12. A. Jenssen, P. Efsing, K. Gott, and P.-O. Andersson, "Crack Growth Behavior of Irradiated Type 304L Stainless Steel in Simulated BWR Environment," in CD, Proc. 11th Intl. Conf. on Environmental Degradation of Materials in Nuclear Power Systems - Water Reactors, Stevenson, WA, Aug. 10-14, 2003, pp. 1015-1026.

13. A. J. Jacobs, G. P. Wozadlo, and G. M. Gordon, "Low Temperature Annealing – A Process to Mitigate IASCC," Corrosion 95, March 26-31, 1995, Orlando, Florida, NACE International, Houston, Texas.

14. A. J. Jacobs and S. Dumbill, "Effects of Low Temperature Annealing on the Microstructure and Grain-Boundary Chemistry of Irradiated 304 SS and Correlation with IASCC," in Proc. 7th Int. Symp. on Environmental Degradation of Materials in Nuclear Power Systems - Water Reactors, August 7-10, 1995, Breckenridge, CO, G. Airey et al., eds., NACE International, Houston, 1995, pp. 1021-1031.

15. S. Katsura, Y. Ishiyama, N. Yokota, T. Kato, K. Nakata, K. Fukuya, H. Sakamoto, and K. Asano, "Post-Irradiation Annealing Effects of Austenitic SS in IASCC," Corrosion 98, NACE International, Houston, TX, 1998, Paper #0132.

16. K. Fukuya, M. Nakano, K. Fujii, M. Kodama, T. Torimaru," Effects of Post-Irradiation Annealing on Radiation-Induced Material Changes and IASCC Susceptibility in PWR-Irradiated Stainless Steels," in CD-ROM Proc. 11th Intl. Conf. on Environmental Degradation of Materials in Nuclear Power Systems - Water Reactors, Stevenson, WA, Aug. 10-14, 2003, pp. 1153-1163.

17. J. T. Busby, G. S. Was, and E. A. Kenik, "Isolation of the Role of Radiation-Induced Segregation in Irradiation-Assisted Stress Corrosion Cracking of Proton-Irradiated Austenitic Stainless Steels," in CD-ROM Proc. 10th Intl. Conf. on Environmental Degradation of Materials in Nuclear Power Systems - Water Reactors, Aug. 5-9, 2001, Lake Tahoe, Nevada.

18. H. M. Chung, W. E. Ruther, J. E. Sanecki, A. G. Hins, and T. F. Kassner, "Stress Corrosion Cracking Susceptibility of Irradiated Type 304 Stainless Steels," in Effects of Radiation on Materials: 16th Int. Symp., ASTM STP 1175, June 23-25, 1992, Aurora, CO, A. S. Kumar, D. S. Gelles, R. K. Nanstad, and T. A. Little, eds., American Society for Testing and Materials, Philadelphia, 1993, pp. 851-869.

19. H. M. Chung, W. E. Ruther, J. E. Sanecki, and T. F. Kassner, "Grain-Boundary Microchemistry and Intergranular Cracking of Irradiated Austenitic Stainless Steels," in Proc. 6th Intl. Symp. on Environmental Degradation of Materials in Nuclear Power Systems - Water Reactors, August 1-5, 1993, San Diego, CA, R. E. Gold and E. P. Simonen, eds., The Minerals, Metals, and Materials Society, Warrendale, PA, 1993, pp. 511-519.

20. K. Fukuya, S. Shima, K. Nakata, S. Kasahara, A. J. Jacobs, G. P. Wozadlo, S. Suzuki and M. Kitamura, "Mechanical Properties and IASCC Susceptibility in Irradiated Stainless Steel," in Proc. 6th Intl. Symp. on Environmental Degradation of Materials in Nuclear Power Systems - Water Reactors, August 1-5, 1993, San Diego, CA, R. E. Gold and E. P. Simonen, eds., The Minerals, Metals, and Materials Society, Warrendale, PA, 1993,, pp. 565-572.

21. A. J. Jacobs, G. P. Wozadlo, T. Okada, S. Kawano, K. Nakata, S. Kasahara, and S. Suzuki, "The Correlation of Grain Boundary Composition in Irradiated Steel with IASCC Resistance," in Proc. 6th Intl. Symp. on Environmental Degradation of Materials in Nuclear Power Systems - Water Reactors, August 1-5, 1993, San Diego, CA, R. E. Gold and E. P. Simonen, eds., The Minerals, Metals, and Materials Society, Warrendale, PA, 1993, pp. 597-604.

22. M. Kodama, J. Morisawa, S. Nishimura, K. Asano, S. Shima, and K. Nakata, "Stress Corrosion Cracking and Intergranular Corrosion of Austenitic Stainless Steels Irradiated at 323 K," J. Nucl. Mater. 212–215 (1994) 1509.

23. H. M. Chung, W. E. Ruther, J. E. Sanecki, A. G. Hins, N. J. Zaluzec, and T. F. Kassner, "Irradiation–Assisted Stress Corrosion Cracking of Austenitic Stainless Steels: Recent Progress and New Approaches," J. Nucl. Mater. 239 (1996) 61.

24. T. Tsukada, Y. Miwa, H. Nakajima, and T. Kondo, "Effects of Minor Elements on IASCC of Type 316 Model Stainless Steels," in Proc. 8th Int. Symp. on Environmental Degradation of Materials in Nuclear Power Systems - Water Reactors, Aug. 10-14, 1997, Amelia Island, FL, S. M. Bruemmer, ed., American Nuclear Society, La Grange Park, IL, 1997, pp. 795-802.

25. J. M. Cookson, G. S. Was, and P. L. Andresen, "Oxide-Induced Initiation of Stress Corrosion Cracking in Irradiated Stainless Steels," Corrosion 54 (1998) 299.

26. H. M. Chung, J.-H. Park, J. E. Sanecki, N. J. Zaluzec, M. S. Yu, and T. T. Yang, "Cracking Mechanism of Type 304L Stainless Steel Core Shroud Welds," in Proc. 9th Intl. Symp. on Environmental Degradation of Materials in Nuclear Power Systems - Water Reactors, August 1-5, 1999, Newport Beach, CA, S. Bruemmer, P. Ford, and G. Was, eds., The Metallurgical Society, Warrendale, PA, 1999, pp. 973-985.

27. H. M. Chung, "Formation of Microcavities in BWR Core Shroud Welds," in CD-ROM Proc. 10th Intnl. Conf. on Environmental Degradation of Materials in Nuclear Power Systems - Water Reactors, August 5-9, 2001, Lake Tahoe, Nevada.

28. S. Kasahara, K. Nakata, K. Fukuya, S. Shima, A. J. Jacobs, G. P. Wozadlo, and S. Suzuki, "The Effects of Minor Elements on IASCC Susceptibility in Austenitic Stainless Steels Irradiated with Neutrons," in Proc. 6th Intl. Symp. on Environmental Degradation of Materials in Nuclear Power Systems - Water Reactors, August 1-5, 1993, San Diego, CA, R. E. Gold and E. P. Simonen, eds., The Minerals, Metals, and Materials Society, Warrendale, PA, 1993, pp. 615-623.

29. T. Tsukada and Y. Miwa, "Stress Corrosion Cracking of Neutron Irradiated Stainless Steels," in Proc. 7th Int. Symp. on Environmental Degradation of Materials in Nuclear Power Systems - Water Reactors, August 7-10, 1995, Breckenridge, CO, G. Airey et al., eds., NACE International, Houston, 1995, pp. 1009–1018.

30. A. Jenssen and L. G. Ljungberg, "Irradiation Assisted Stress Corrosion Cracking - Postirradiation CERT Tests of Stainless Steels in a BWR Test Loop," in Proc. 7th Int. Symp. on Environmental Degradation of Materials in Nuclear Power Systems - Water Reactors, August 7-10, 1995, Breckenridge, CO, G. Airey et al., eds., NACE International, Houston, 1995, pp. 1043–1052.

31. S. Dumbill, "Examination of Stress Corrosion Crack Tip Microstructures in Stainless Steel," SKI Report 01:35, Swedish Nuclear Power Inspectorate, September 2001.

32. S. Bruemmer and L. Thomas, "Stress Corrosion Crack-Tip Characteristics in Austenitic Stainless Steels Exposed to High-Temperature Water Environments," Handout presented at the International Cooperative Group on Environmentally Assisted Cracking, Kyungju, South Korea, April 2001.

33. L. Thomas and S. Bruemmer, "Analytical Transmission Microscopy (ATEM) Characterization of Stress Corrosion Cracks in LWR-Irradiated Austenitic Stainless Steel Components," EPRI-1003422, Electric Power Research Institute, Palo Alto, CA, May 2002.

34. L. Thomas and S. Bruemmer, "Analytical Transmission Microscopy (ATEM) Characterization of Stress Corrosion Cracks in LWR-Irradiated Austenitic Stainless Steel Components," in CD-ROM Proc. 11th Intl. Conf. on Environmental Degradation of Materials in Nuclear Power Systems - Water Reactors, Stevenson, WA, Aug. 10-14, 2003, pp. 1049-1061.

35. G. Taguchi, in "Quality Engineering Using Robust Design," M. S. Phadke, ed., Prentice Hall, Englewood Cliffs, NJ, 1989.

36. H. M. Chung, R. V. Strain, and W. J. Shack, "Irradiation-Assisted Stress Corrosion Cracking of Model Austenitic Stainless Steels," in Proc. 9th Intl. Symp. on Environmental Degradation of Materials in Nuclear Power Systems - Water Reactors, August 1-5, 1999, Newport Beach, CA, S. Bruemmer, P. Ford, and G. Was, eds., The Metallurgical Society, Warrendale, PA, 1999, pp. 931-939.

37. H. M. Chung, W. E. Ruther, and R. V. Strain, "Irradiation-Assisted Stress Corrosion Cracking of Model Austenitic Stainless Steels Irradiated in the Halden Reactor," NUREG/CR-5608, ANL-98/25, Argonne National Laboratory, March 1999.

38. H. M. Chung, R. V. Strain, and W. J. Shack, "Irradiation-Assisted Stress Corrosion Cracking of Model Austenitic Stainless Steel Alloys," in CD-ROM Proc. 10th Intl. Conf. on Environmental Degradation of Materials in Nuclear Power Systems - Water Reactors, Aug. 5-9, 2001, Lake Tahoe, Nevada.

39. H. M. Chung, W. E. Ruther, R. V. Strain, and W. J. Shack, "Irradiation-Assisted Stress Corrosion Cracking of Model Austenitic Stainless Steel Alloys," NUREG/CR-6687, ANL-00/21, Argonne National Laboratory, October 2000.

40. H. M. Chung, R. V. Strain, D. L. Perry, and W. J. Shack, "Irradiation-Assisted Cracking of Austenitic Stainless Steels in Water and in Inert Environment," in CD-ROM Proc. 11th Intl. Conf. on Environmental Degradation of Materials in Nuclear Power Systems - Water Reactors, Stevenson, WA, Aug. 10-14, 2003, pp. 1164-1175.

41. Y. Tanaka, S. Suzuki, K. Fukuya, H. Sakamoto, M. Kodama, S. Nishimura, K. Nakata, and T. Kato, "IASCC Susceptibility of Type 304, 304L and 316 Stainless Steels," in Proc. 8th Int. Symp. on Environmental Degradation of Materials in Nuclear Power Systems - Water Reactors, , Aug. 10-14, 1997, Amelia Island, FL, S. M. Bruemmer, ed., American Nuclear Society, La Grange Park, IL, 1997, pp. 803-811.

42. F. Garzarolli, P. Dewes, R. Hahn, and J. L. Nelson, "In-Reactor Testing of IASCC Resistant Steels," in Proc. 7th Int. Symp. on Environmental Degradation of Materials in Nuclear Power Systems - Water Reactors, August 7-10, 1995, Breckenridge, CO, G. Airey et al., eds., NACE International, Houston, 1995, pp. 1055–1065.

43. A.-T. Shen and C. S. Chang, "IASCC Behavior of 304L Stainless Steel," in CD-ROM Proc. 11th Intl. Conf. on Environmental Degradation of Materials in Nuclear Power Systems - Water Reactors, Stevenson, WA, Aug. 10-14, 2003, pp. 986-994.

44. J. M. Cookson, D. L. Damcott, G. S. Was, and P. L. Anderson, "The Role of Microchemical and Microstructural Effects in the IASCC of High-Purity Austenitic Stainless Steels," in Proc. 6th Intl. Symp. on Environmental Degradation of Materials in Nuclear Power Systems - Water Reactors, August 1-5, 1993, San Diego, CA, R. E. Gold and E. P. Simonen, eds., The Minerals, Metals, and Materials Society, Warrendale, PA, 1993, pp. 573-580.

45. J. T. Busby and G. S. Was, "Irradiation-Assisted Stress Corrosion Cracking in Model Austenitic Alloys with Solute Additions," in CD-ROM Proc. 11th Intl. Conf. on Environmental Degradation of Materials in Nuclear Power Systems - Water Reactors, Stevenson, WA, Aug. 10-14, 2003, pp. 995-1014.

46. T. M. Karlsen and E. Hauso, "Qualification and Application of Instrumented Specimens for In-Core Studies on Cracking Behavior of Austenitic Stainless Steels," in Proc. 9th Intl. Symp. on Environmental Degradation of Materials in Nuclear Power Systems - Water Reactors, August 1-5, 1999, Newport Beach, CA, S. Bruemmer, P. Ford, and G. Was, eds., The Metallurgical Society, Warrendale, PA, 1999, pp. 951-961.

47. M. Hansen, "Constitution of Binary Alloys," McGraw Hill, New York, 1958, pp. 704-707.

48. A. J. Jacobs, R. E. Clausing, M. K. Miller, and C. Shepherd, “Influence of Grain Boundary Composition on the IASCC Susceptibility of Type 348 Stainless Steel,” in Proc. 4th Intl. Conf. on Environmental Degradation of Materials in Nuclear Power Systems - Water Reactors, Stevenson, WA, Aug. 10-14, 2003, pp. 14-21 to 14-44.

49. P. L. Andresen and C. L. Briant, "Role of S, P, and N Segregation on Intergranular Environmental Cracking of Stainless Steels in High Temperature Water," in Proc. 3rd Intl. Symp. on Environmental Degradation of Materials in Nuclear Power Systems – Water Reactors, August 30-September 3, 1987, Traverse City, MI, G. J. Theus and J. R. Weeks, eds., The Metallurgical Society, Warrendale, PA, 1988, pp. 371-381.

50. J. K. Heuer, P. R. Okamoto, N. Q. Lam, J. F. Stubbins, “Disorder-Induced Melting in Nickel: Implication to Intergranular Sulfur Embrittlement,” J. Nucl. Mater. 301 (2002) 129-141.

51. P. R. Okamoto, J. K. Heuer, and N. Q. Lam, "Is Segregation-Induced Grain Boundary Embrittlement a Polymorphous Melting Process?" in CD-ROM Proc. 2003 TMS Spring Meeting, March 2-6, 2003, San Diego, California, NACE International, Houston, Texas.

52. K. Hide, T. Onchi, M. Mayazumi, and S. Dumbill, “Correlation of Microstructure and IGSCC Behavior for Irradiated Thermally Sensitized Type 304 Stainless Steels,“ in CD-ROM Proc. 10th Intl. Conf. on Environmental Degradation of Materials in Nuclear Power Systems - Water Reactors, Aug. 5-9, 2001, Lake Tahoe, Nevada.

53. T. Onchi, K. Dohi, and N. Soneda, “Neutron Fluence Dependent Intergranular Cracking of Thermally Sensitized Type 304 Stainless Steel at 290°C in Inert Gas and in Water,” in CD-ROM Proc. 11th Intl. Conf. on Environmental Degradation of Materials in Nuclear Power Systems - Water Reactors, Stevenson, WA, Aug. 10-14, 2003, pp. 1111-1120.

54. H. M. Chung, J.-H. Park, W. E. Ruther, J. E. Sanecki, R. V. Strain, and N. J. Zaluzec, “Stress Corrosion Cracking Of Austenitic Stainless Steel Core Internal Welds,” Corrosion '99, April 25-30, 1999, San Antonio; Paper No. 443.

55. H. M. Chung, D. L. Perry, and W. J. Shack, "Sulfur in Austenitic Stainless Steel and Irradiation-Assisted Stress Corrosion Cracking," Corrosion 2003, March 16-20, San Diego, CA, Paper #3662.

56. Proc. Intl. Symposium on: "Sulfide Inclusions in Steel," November 7-8, 1974, Port Chester, New York, J. J. de Barbadillo and E. Snape, eds., American Society of Metals, Warrendale, Pennsylvania.

57. H. M. Chung, J. E. Sanecki, and F. A. Garner, "Radiation–Induced Instability of MnS Precipitates and Its Possible Consequences on Irradiation–Induced Stress Corrosion Cracking of Austenitic Stainless Steels," in Effects of Radiation on Materials: 18th Intl. Symp., June 23-25, 1996, Hyannis, MA, ASTM STP 1325, R. K. Nanstad, M. L. Hamilton, A. S. Kumar, and F. A. Garner, eds., American Society for Testing and Material, 1999, pp. 647-658.

58. M. F. Ashby and F. Spaegen, “A New Model for the Structure of Grain Boundaries: Packing of Polyhedra,” Scripta Met. 12 (1978) 193.

NRC FORM 335
(9-2004)
NRCMD 3.7

U. S. NUCLEAR REGULATORY COMMISSION

BIBLIOGRAPHIC DATA SHEET

(See instructions on the reverse)

1. REPORT NUMBER
(Assigned by NRC. Add Vol., Supp., Rev., and Addendum Numbers, if any.)

NUREG/CR–
ANL—04/10

2. TITLE AND SUBTITLE

Irradiation-Assisted Stress Corrosion Cracking Behavior of Austenitic Stainless Steels Applicable to LWR Core Internals

3. DATE REPORT PUBLISHED

MONTH	YEAR
March	2005

4. FIN OR GRANT NUMBER

Y6388

5. AUTHOR(S)

H. M. Chung and W. J. Shack

6. TYPE OF REPORT

Technical; Topical

7. PERIOD COVERED (Inclusive Dates)

8. PERFORMING ORGANIZATION – NAME AND ADDRESS *(If NRC, provide Division, Office or Region, U.S. Nuclear Regulatory Commission, and mailing address; if contractor, provide name and mailing address.)*

Argonne National Laboratory
9700 South Cass Avenue
Argonne, IL 60439

9. SPONSORING ORGANIZATION – NAME AND ADDRESS *(If NRC, type "Same as above": if contractor, provide NRC Division, Office or Region, U.S. Nuclear Regulatory Commission, and mailing address.)*

Division of Engineering Technology
Office of Nuclear Regulatory Research
U.S. Nuclear Regulatory Commission
Washington, DC 20555–0001

10. SUPPLEMENTARY NOTES

William H. Cullen, Jr., NRC Project Manager

11. ABSTRACT (200 words or less)

As LWRs age and neutron fluence increases, core internals become susceptible to irradiation-assisted stress corrosion cracking (IASCC). To better understand the mechanism of this type of degradation, austenitic stainless steels were irradiated in the Halden reactor under BWR conditions, and slow-strain-rate tensile tests were conducted in BWR-like water on 27 commercial and model laboratory heats. Fractographic and microchemical analyses were performed to characterize grain-boundary segregation of alloying and impurity elements. As neutron damage increases to ≈3 dpa, sulfur atoms play a dominant role in causing IASCC. To provide good resistance to IASCC in Types 304 or 316 steel, it is necessary to ensure a sulfur content of <0.002 wt.% and a carbon content of >0.03 wt.%. A two-dimensional map was developed in which IASCC susceptibility or resistance of Types 304 or 316 is shown as a function of bulk concentrations of S and C. A similar map is applicable to Type 348 steel. Nine heats of Types 304, 316, and 348 steel were identified to be resistant to IASCC under BWR conditions. On the basis of the results of the stress-corrosion-cracking tests and the microstructural characterization, a mechanistic IASCC model was developed.

12. KEY WORDS/DESCRIPTORS *(List words or phrases that will assist researchers in locating this report.)*

Irradiation-induced degradation
Stress corrosion cracking
BWR core internals
Grain boundary segregation

13. AVAILABILITY STATEMENT
unlimited

14. SECURITY CLASSIFICATION
(This Page)
unclassified

(This Report)
unclassified

15. NUMBER OF PAGES
101

16.PRICE